2019-01-24

Mapping shrub biomass in a boreal continental fen

He, Annie

UNIVERSITY OF CALGARY

Mapping shrub biomass in a boreal continental fen

by

Annie He

A THESIS

SUBMITTED TO THE FACULTY OF GRADUATE STUDIES

IN PARTIAL FULFILMENT OF THE REQUIREMENTS FOR THE

DEGREE OF MASTER OF SCIENCE

GRADUATE PROGRAM IN GEOGRAPHY

CALGARY, ALBERTA

JANUARY, 2019

Abstract

Biomass estimation is a heavily explored topic in the literature, as biomass information can provide valuable insight into understanding an ecosystem's health. However, few studies exist on quantifying aboveground biomass (AGB) in peatlands. This thesis summarizes how allometric equations and unmanned aerial vehicles (UAV) can be used to map AGB across a 2-hectare peatland site. Prior to using UAVs to measure AGB, accurate field measurements are required to calibrate and validate the UAV-AGB model. We developed allometric equations for three dominant shrub genera found in boreal peatlands and found that equations based on shrub genus were not significantly different from a pooled equation of all shrub genera. The UAV study revealed that UAV-derived volume was the best predictor of AGB (R^2=0.885) and was subsequently used as the dependent variable for our AGB model. This thesis reports the findings revealed through the process of estimating AGB using allometric equations and UAVs.

Preface

This is a manuscript-based thesis prepared in accordance with the Faculty of Graduate Studies Guidelines at the University of Calgary. I was responsible for the research design, data collection, analysis and writing in this thesis. Chapter 2 was published by MDPI in the open-access, peer-reviewed journal *Forests*. The research presented in Chapter 2 was primarily completed by myself. My coauthors (Dr. Gregory McDermid, Dr. Mir Mustafizur Rahman, Dr. Maria Strack, Dr. Bin Xu, and Saraswati Saraswati) provided feedback on my research design, interpretation of results and assisted with editing my final manuscript. Dr. Tak Fung, with the University of Calgary, assisted with the statistical analysis presented in Chapter 2 and my field assistant, Bret Collins, assisted with the data processing. Chapter 3 will be submitted to a peer-reviewed journal at a later date. Chapter 3 was primarily completed by myself with the assistance of Dr. Gregory McDermid and Dr. Mir Mustafizur Rahman who provided support with research design and editing of the final manuscript.

The amount of biomass estimation studies found in peatlands is scant. Chapter 2 and Chapter 3 represents two different biomass estimation approaches that have been applied to the same peatland site. The research published in this thesis aims to address the identified research gap within the literature. The full citations are as follows:

He, A., McDermid, G., Rahman, M., Strack, M., Saraswati, S., & Xu, B. (2018). Developing Allometric Equations for Estimating Shrub Biomass in a Boreal Fen. *Forests*, *9*(9), 569.

Acknowledgements

This work would not have been possible without the support from friends, family, and the F^{3}GISci team. I would like to thank my supervisor, Dr. Gregory McDermid, who offered me a place in his lab and on the peatland project. His advice helped me navigate through all challenges, technical and interpersonal, with as little resistance as possible. I am very grateful for his support and the trust he placed in my abilities. Dr. Mir Mustafizur Rahman, my co-supervisor, was also instrumental with his constant encouragement and accountability to ensure I would honor my timelines.

I was fortunate to have receive input from Dr. Bin Xu and Dr. Maria Strack from the start of my research. I would like to thank Dr. Bin Xu for his assistance with my fieldwork and for juggling all the administrative details that allowed for my fieldwork to be conducted with ease. I am appreciative of Dr. Maria Strack for sharing her expertise with me and always being available for questions. I would also like to thank Dr. John Robert Post for his willingness to serve on my thesis review committee as my external internal examiner.

The words I have expressed here are a small fraction of the appreciation I feel for all the people who have journeyed with me through my research over the past two years. Each person I have encountered has guided me and encouraged me in some way to get me to where I am today. Kevin and the Ark of Christ Victory Church have been instrumental in my personal spiritual growth through this process. I am also very grateful for the unconditional love and support received from my mom and sister. Last, but not least, I know that none of this would be possible without God, my Lord and Savior, who has walked with me through each obstacle and shown me that His love is enough.

For mom, who continues to amaze me with your strength and perseverance over the years. Thank you for being a great example of strength and hard work.

Table of Contents

List of Tables

List of Figures

List of Symbols, Abbreviations and Nomenclature

Abbreviation	**Definition**
AGB	Aboveground biomass
CH_4	Methane
CHM	Canopy Height Model
CO_2	Carbon Dioxide
DPC	Dense Point Cloud
DSM	Digital Surface Model
DTM	Digital Terrain Model
ERA	Emissions Reduction Alberta
GHG	Greenhouse Gas
GCP	Ground Control Points
N	Number of samples
NDVI	Normalized Difference Vegetation Index
N_2O	Nitrous Oxide
R^2	Coefficient of Determination
RMSE	Root Mean Squared Error
RSS	Residual Sum of Squares
SE	Standard Error
SR	Simple Ratio
SfM	Structure from Motion
TM	Thematic Mapper
UAV	Unmanned Aerial Vehicle
VI	Vegetation Indices

Chapter One: Introduction

1.1 Background

Peatlands are wetlands that have accumulated a thick layer of organic material, referred to as peat, over thousands of years. According to the Alberta Wetland Classification system, wetlands are defined as land that has been saturated with water long enough to have altered the vegetation, soils, and other kinds of biological activity (ESRD, 2015). Peatlands are one of the two types of wetlands, the other type being mineral wetlands. In Alberta, peatlands are distinguished by the presence of at least 40 cm of accumulated peat of which must be almost entirely organic matter and be undecomposed (ERSD, 2015). The formation of this peat ensues in ecosystems where the biomass production rate is higher than the decomposition rate (Vitt, 2006). Peatlands are largely found in the northern boreal forest characterized by a cold-temperate boreal climate (Wieder & Vitt, 2006). The excess water and the low temperatures, found in this region, prevent the complete decay of biomass which results in the formation of peat (Charman, 2002).

The northern boreal forest covers 1.9 billion hectares of the Earth's surface, with 28% being located in Canada (Natural Resources Canada, 2018). Peatlands cover 12% of the Canadian landscape, with the majority of peatlands found in the Hudson Bay lowlands and the Mackenzie River Basin (Vitt, 2006).

Peatlands are generally classified into fens and bogs; fens receive water from a variety of sources whereas bogs receive water from precipitation (ESRD, 2015). Generally, bogs have more acidic water compared to fens with a pH of less than 4.5 (ERSD, 2015). Fens have a pH of greater than 4.5, however, it can be lower depending on the groundwater flow (ERSD, 2015). The type of peatland initiated is dependent on local climate, regional substrate, water chemistry, and therefore there can be a wide variety of peatlands types (Vitt et al., 2003). The Hudson Bay Lowlands are predominantly composed of fens whereas the Mackenzie River Basin has permafrost bogs in the north and fen complexes in the south. The Hudson Bay lowlands are located between the Canadian Shield on the eastern side of the country covering the province of Ontario with smaller portions reaching into Manitoba and Quebec. The Mackenzie River Basin covers five provinces: British Columbia, Alberta, Saskatchewan, Yukon and the Northwest Territories. In the Hudson Bay Lowlands, most peatlands are open and treeless (Munir et al., 2014) whereas the Mackenzie River Basin peatlands have more trees. The relatively drier climate found in the Mackenzie River Basin is one of the reasons for the presence of trees (Vitt & Bhatti, 2012).

In Alberta, wetlands in the southern region of the province are largely mineral wetlands whereas peatlands are dominant in the northern regions (AEP, 2014). Fens account for 60% of total wetland coverage in continental Canada (Miller et al., 2015) and approximately 65% of the region's peatland carbon is found in fen peat (Vitt et al., 2000). Comparatively, bogs cover relatively less area and have a lower carbon density (Vitt et al., 2009). Fens, across continental Canada, can be highly variable in chemistry, structure and flora (Vitt et al., 2009) because of the various landscape positions fens are situated within (ERSD, 2015). Fens are further classified into three groups based on the acidity and alkalinity gradient: 1) poor fens, 2) moderate-rich fens, and 3) extreme-rich fens. Poor fens are found in Alberta's northern highlands or in areas where surface water inputs are acidic, moderate-rich fens are found in close proximity to coarse-grained surficial deposits and extreme-rich fens can be found in northeastern Alberta on glaciofluvial deposits (ERSD, 2015). There is less variation in continental bogs compared to those found in fens. Bogs in Alberta have a permafrost layer and are characterized by sphagnum mosses with some true mosses, ericaceous shrubs, and black spruce trees (Wieder et al., 2009). Bogs are also classified into three groups: 1) treed bogs, 2) shrubby bogs, and 3) open bogs. In Alberta's boreal zone, treed bogs are the dominant type of bogs.

1.1.1 The global significance of peatland

Peatlands contribute to the global carbon cycle by acting as a global carbon sink-storing ~33% of the world's soil carbon while only covering 3% of the world's surface (Wieder & Vitt, 2006). The process of photosynthesis enables the conversion of atmospheric carbon to carbon rich carbohydrates and sugars that are stored in plants; the carbon is only released back into the atmosphere as carbon dioxide (CO_2) after the plants have decomposed (Kuzyakov & Gavrichkova, 2010). In a peatland system, carbon remains stored in the organic material for longer because the colder climate and saturated soil causes decomposition to occur at a slower rate (Brinson et al., 1981; Bartsch and Moore

1985). For these reasons, peatlands have been commonly referred to as an unbalanced system (Vitt, 2006).

Methane (CH_4) is another greenhouse gas that is commonly mentioned in the discussion of peatlands. Peatlands are a net source of CH_4 with an annual release that accounts for 12.2% of the total global emission rate (Wuebbles and Hayhoe, 2002). The oversaturated soils and anoxic environment, which promote the slower decomposition rates, also enables the production of methane gas (Lai, 2009). Methane is produced in the anaerobic zone of soils through the process of methanogenesis by methanogens, which are microbes that can only survive in the absence of oxygen (Lai, 2009). Some of this methane can be consumed or oxidized into carbon dioxide in the aerobic zone by methanotrophic bacteria. However, if the oxic zone is very small or water table depth is low in peatland soils, then consumption of methane is minimal and methane gas is released (Lai, 2009).

Peatlands operate on a fine balance, where any changes to the climate or landscape could alter the ecosystem function (Miller et al 2015). Despite the global importance of monitoring peatlands, knowledge on how disturbances may affect the carbon and methane exchange in these ecoregions is limited (Turetksy et al., 2011; Miller et al., 2015; Strack et al., 2018). In addition, northern peatlands exhibit high spatial, climatic, and micro-topographic variation across peatland types. Each peatland will react uniquely to disturbances, making it difficult to estimate the magnitude of regional CH_4 and CO_2 fluxes (Lai, 2009). Changes to CO_2 and CH_4 balances in peatlands could potentially generate feedback effects that have the potential to enhance global greenhouse warming (Joabsson et al., 1999). The next section will discuss the two major threats to northern peatlands.

1.1.2 Peatlands and climate change

Climate change studies have predicted that the northern regions will experience the largest impacts of climate change; this is also where majority of peatlands are located (Tarnocai et al 2006; IPCC, 2007). The predicted annual increase of temperature by the Canadian Global Climate Model is a 3-4 degrees Celsius increase in mean annual temperature by 2020, with the greatest temperature increase in the winter months (Hengeveld, 2000). A rise in temperature could have a significant impact on peatlands as their functioning is largely controlled by changes in climate (Vitt, 2006). Any changes to climatic conditions can affect the development and stability of peatland carbon stock (Christensen et al 2007) and the overall methane release rates (Bridgeham et al 2013; Turetsky et al 2014). For example, rising air temperatures can lead to warmer and drier conditions of the soil, earlier start to the growing season (Moore et al., 1998), increased litter decomposition rates (Moore et al., 1999), and the lowering of water table, which can all contribute to increased CO_2 emission rates (Moore and Dalva, 1993; Silvola et al., 1996).

The response of CH_4 flux is dependent on how climatic change will affect the microbial environment which is largely dependent on changes to the water table position (Moore et al 1998). Climate change will have varying effects across northern peatlands because of the variability in vegetation and water table (Moore et al., 1998). For example, in Canada, Moore et al. (1998) predicted an increase in CH_4 emissions in northern regions and a decrease in southern regions. Information on how these peatlands are responding to climate change can be extremely valuable for measuring global greenhouse gas emissions.

1.1.3 Peatlands and Anthropogenic changes

In addition to climate change, peatlands have also experienced high volume of human disturbances which have impacted their ecosystem functioning (Strack et al., 2018). As of 2003, human actions have exploited a total of 500 000 km^2 of active peatlands in northern regions (Chapman et al., 2003). Land changes have been caused by agriculture (Fargione et al., 2008; Knox et al., 2015), forestry (Lieffers & Macdonald,1990), peat harvesting (Lai, 2009), and oil and gas extraction (Turetsky et al., 2011; Yeh et al., 2009). All these activities require changes to the landscape that can affect the local hydrology, ecosystem function, rates of peat accumulation, vegetation changes, and greenhouse gas flux (Turetsky et al., 2011).

1.1.3.1 The impact of linear disturbances on Canadian peatlands

Canadian peatlands, specifically in Alberta, are undergoing major changes with climate change as well as the vast development of oil infrastructure in the northern boreal (Alberta Energy, 2011). Between 2000-2005, Alberta's oil sands region was one of the hotspots of global forest cover loss (Hansen et al 2010) primarily attributed to oil and gas exploration (Government of Alberta, 2012). Generally, oil and gas exploration require the clearing of land, construction of infrastructure, peatland drainage, and other potentially destructive activities. These activities can result in reducing carbon uptake by the tree biomass (Strack et al 2018), lowering of water table (Turetsky et al., 2011), and flooding or damming across the linear features (Patterson and Cooper, 2007), all of which could lead to the release of large volumes of carbon (Wieder & Vitt, 2006; Strack et al., 2006; Munir et al., 2014).

Linear disturbances, such as roads, seismic lines, and pipelines, are a major concern for Albertan peatlands because they are expected to quadruple within the next century if current economic practices are to continue (Turetsky et al., 2011)(Figure 1.2). Pasher et al. (2013) estimated that linear disturbances accounted for 80% of boreal anthropogenic disturbance. Some studies have studied how linear disturbances can affect hydrology (Braverman & Quinton, 2016; Patterson and Cooper, 2007) and vegetation (Miller et al., 2015). Braverman & Quinton (2016) and Patterson and Cooper (2007) found that the construction of seismic lines (Braverman & Quinton, 2016) and mineral soil fill road (Patterson and Cooper, 2007) caused flooding. Miller et al (2015) found that long-term drying resulted in a two- to four-fold increase in total biomass in three of four fen sites (Miller et al., 2015). The drying also, consequently, resulted in a reduction in understory (Miller et al., 2015). Information on the potential hydrologic and vegetative changes caused by linear disturbances has been documented, however, less research is found on how these changes will affect greenhouse gas emissions (Strack et al., 2017).

***Figure 1.1**: Field photos taken of a Canadian bog located in northern Alberta. One photo shows a mineral soil fill road (top) and the other photo shows a seismic line (bottom).*

My thesis contributes to the The Improved Construction of Roads and Pipelines to Minimize Impact on Peatland Greenhouse Gas Emissions Project funded by Emissions Reduction Alberta (ERA). The goals of this larger project are to determine the impact of current permanent linear disturbances on peatland greenhouse gas emissions and to assess the impact of culverts and their potential in reducing emissions. Permanent linear disturbances, in this case, refer to linear disturbances which mineral soil fill has been placed. An understanding of how peatlands are affected by these disturbances can provide future developers with a better understanding of the impact of these disturbances and how to minimize adverse effects. The study sites are located near Peace River, AB within Canadian Natural Resources (CNRL)'s Carmon Creek in situ oil sands lease. The project has a local and regional component; to determine local impact, closed chamber methods will be used to determine ground layer fluxes of CO_2, CH_4, and N_2O (nitrous oxide). Remote sensing will be used to assess regional impact by measuring three biophysical parameters: microtopography, ground water levels, and biomass. These three biophysical parameters have been identified as relevant in estimating greenhouse gas emissions. Our approach links greenhouse gas flux to land-cover type, depth to water table, and biomass through empirical estimates derived at local field sites. Information on microtopography (Lovitt et al., 2017) and ground water table (Rahman et al., 2017) have previously been published. Biomass is the remaining information required for the completion of this project, which this thesis will address.

1.2 Biomass Estimation

Biomass is defined as the total weight of organic matter and includes the weight above and below ground (Song, 2013) such as trees, shrubs, vines and roots (Lu, 2006). Majority of biomass estimation studies focus on aboveground biomass because belowground biomass is difficult to measure (Lu et al., 2016). Consequently, in this thesis, the term "biomass" will be used to represent only aboveground biomass (AGB) unless stated otherwise.

Biomass estimates provide information on 1) local carbon stock (Paul et al., 2016; Le Toan et al., 2011), 2) water table position (Couwenberg et al., 2011), and 3) methane flux (Joabsson et al., 1999). Accurate biomass estimates can also significantly reduce uncertainties of carbon emission and sequestration (Foody, 2003; (Crawford and Bluestein, 2000; Schaudt and Dickinson, 2000). Information on water table depth is reflected in biomass, as the two are interdependent (Miller et al., 2015). A higher water table will create more anoxic conditions which limits the oxygen availability for plants and decrease plant productivity whereas a water table drawn-down leads to increased plant productivity (Munir et al., 2014; Lieffers and Rothwell, 1987). Vascular plants are also key factors in controlling processes coupled to transport, production, and consumption of methane, therefore, biomass information has also been used as a proxy to predict the levels of methane emissions (Joabsson et al., 1999; Dias et al., 2010).

1.2.1 Biomass estimation in peatlands

Biomass estimation is a heavily explored topic in the literature, however, studies done in peatlands are scarce. The vegetation found across different peatland types can be highly variable. Peatlands are generally classified based on climate, hydrology, chemistry, substrate, and vegetation/flora (Vitt, 2006). Generally, peatlands are considered hostile places for plant life because they are waterlogged, there is poor nutrient and oxygen availability, high acidity, and high availability of toxins (e.g. sulphur, iron, and manganese) (Charman, 2002). The combination of these conditions causes for many peatland plants to be nutritionally impoverished and therefore have low growth rates (Vitt, 2006).

Biodiversity is also considered low because most plants have not adapted to these harsh conditions (Vitt, 2006).

Shrubs are multi-stemmed woody plants that can account for up to 88% of total AGB in the Canadian continental boreal peatlands, based on Campbell et al (2000)'s synthesis. Shrub biomass can range from 10.0 g m-2 (grams per squared meter) for non-permafrost bogs to 11 903.0 g m-2 in a shrubby moderately rich fen (Campbell et al., 2000). Figure 1.3 is a comparison of the percentages of vegetation coverage for three different types of peatlands. It shows how vegetation can vary across different peatland types.

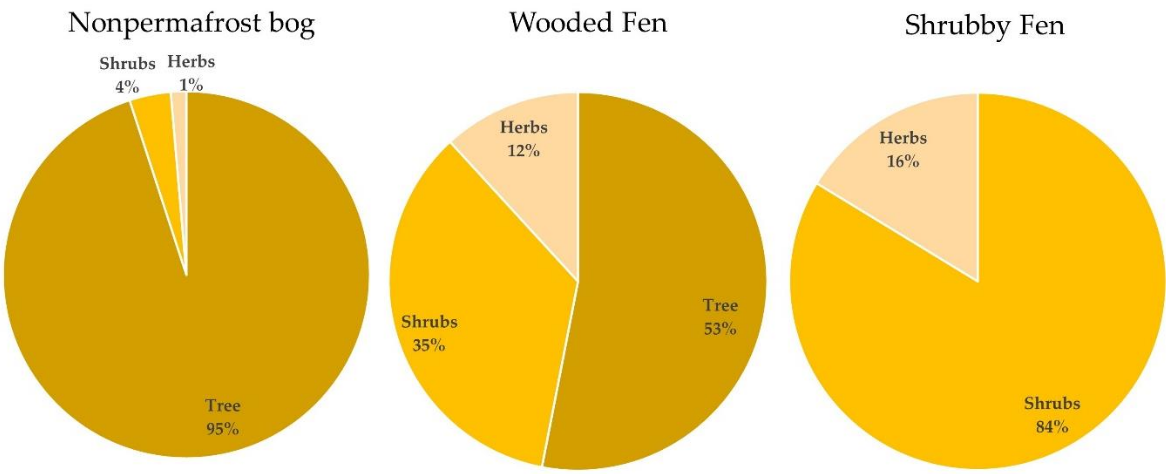

Figure 1.2*: Pie graphs of the percentage of the vegetation coverage for three different peatland types taken from data gathered by Campbell et al. (2000). Moss biomass was not gathered in this report; therefore, it is not included in these charts.*

Shrub biomass is not of high interest to foresters, as they are generally considered non-merchantable. Consequently, relatively fewer biomass-estimation studies have been conducted in sites that are dominated by shrubs, like fens. Amongst the few biomass estimation studies completed in peatlands, the most popular techniques are 1) allometric models and 2) remote sensing.

1.2.1.1 Allometric models developed in peatlands

Allometric models are an alternative to destructive sampling, as destructive sampling is expensive and time-consuming (Verwijist & Telenius, 1999; Lu et al., 2016) (Figure 1.4). Allometric models use one or more plant dimension (e.g. stem diameter, diameter at breast height) to estimate a separate dimension that is more difficult to obtain (e.g. stem volume, biomass). Unlike direct measurement (or destructive sampling), the development of allometric models require the performance of complex analysis and mathematical operations and are therefore not as accurate because generalizations are made. Direct measurements of biomass, however, are limited to small areas due to time and labor restraints whereas once allometric models are developed, they can be used quickly and non-destructively for stand biomass inventories (Lu et al., 2016). Caution does need to be exercised when applying allometric equations outside of the region where they were developed (Clark and Kellner, 2012; Lu et al., 2016) and when equations are generalized beyond the species level (Paul et al, 2013).

Conolly and Grigal (1983) and Brand & Smith (1985) were the only allometric studies found for shrubs in wetlands. In both studies, their models achieved good predictive capacity for estimating aboveground biomass (R^2 = 0.83 - 0.96). Bond-Lamberty (2002) also developed allometric equations across 17 study sites in boreal forests near Thompson, Maine. However, the equations they developed were for larger tree species (Bond-Lamberty et al., 2002).

***Figure 1.3**: Field photos taken of field assistant, Bret Collins collecting shrubs in a boreal continental fen to be used for the development of allometric models.*

1.2.1.2 Remote sensing applied in peatlands

Remote sensing is another popular method used for biomass estimation (Lu et al., 2016). Unlike field-based methods (e.g. allometric models), remote sensing methods offer the capability of capturing land surface features over large areas using airplanes or satellites (Lu et al., 2016; Lucas et al., 2015; Song et al, 2013). Optical, radar, and lidar sensors have all been used within the biomass estimation literature with each sensor offering its own comparative advantage. The type of platform or sensor that is most effective in biomass estimation is largely dependent on the availability of data for the area of interest and the type of vegetation coverage (dense, sparse, etc.). A popular analytical method, regardless of sensor, is the use of empirical models to estimate biomass by finding the most accurate predictor variable. Optical sensors typically use spectral bands or vegetation indices (VI), radar uses backscatter values (Englhart et al., 2011; Peregon & Yamagata, 2013), and lidar uses structural variables such as canopy height (Hopkinson et al., 2005; Bendig et al., 2015).

Amongst the three peatland-biomass studies that were found, two studies used radar backscatter values to estimate aboveground biomass (Englhart et al., 2011; Peregon & Yamagata, 2013) and one used lidar (Hopkinson et al 2005). The benefit of radar sensors is that they can penetrate beneath the forest canopy and are not affected by weather or daylight (Englhart et al., 2011). Both studies used backscatter values to achieve a R^2 of 0.49 and 0.53, respectively. A major limitation with using radar data is data saturation; radar has been found to be less useful in complex canopies and higher biomass forests (Le Toan et al., 2004; Peregoon & Yamagata, 2013). Hopkinson et al (2005) used lidar for measuring canopy height and vegetation class in a boreal wetland. They found that, despite a systematic underestimation of height for all vegetation classes, the lidar canopy surface height was significantly correlated with measured heights at the 99% confidence level. They also noticed that the largest errors were associated with low shrub (< 2m) and aquatic vegetation (Hopkinson et al., 2005).

A platform that has yet to be explored in peatland biomass estimation is Unmanned Aerial Vehicles (UAVs). UAVs are remotely controlled drones capable of carrying a variety of sensors. UAVs have a relatively low flight height which allow for the collection of high-density data at a significantly lower surveying cost compared to full-scale lidar platforms (Fraser et al., 2016). Different sensors can also be mounted to UAVs; however, optical cameras are most commonly used. In addition to spectral information, structural information can also be gathered through the generation of a 3D model based on principles of photogrammetry. Structure-from-Motion (SfM) and computer software is used to stich optical images together based on similar features found across overlapping images; the amount of overlap between each image can be specified by the user and determines the number of photos captured. Once all the images are oriented, the software is able to recognize similar points across overlapping images and the distances between key features are calculated. From here, the construction of the dense point cloud begins which results in the generation of a 3D model of the site. The data collected from UAVs can be used to generate orthophotographs that can used for vegetation classification.

UAVs have been used successfully in a number of biomass estimation studies in other ecoregions such as standing crops (Bendig et al., 2014; Yue et al., 2017), woodlands (Puliti et al., 2015), and arctic tundra (Tommervik et al., 2014; Mora et al., 2015; Fraser et al., 2016). The challenges associated with mapping arctic shrubs is similar to those with mapping peatland shrubs; for example, there can be low variation in vegetation height and peatland shrubs are also of low stature which can be missed by coarse and moderate resolution sensors (Kulawardhana et al., 2014). High density data would improve one’s ability to map these low-stature shrubs. We believe that UAVs offer that high resolution required to capture the shrubs as Fraser et al. (2017) was able to demonstrate: that UAVs could even be used to detect a < 10 cm change in vegetation height the low-lying artic shrubs.

1.3 Statement of the problem

The impact of climate change and linear disturbances and how it may affect Alberta's peatlands is poorly understood. These changes could potentially trigger greenhouse gas emissions, specifically CO_2 and CH_4. The Improved Construction of Roads and Pipelines to Minimize Impact on Peatland Greenhouse Gas Emissions Project aims to help address this knowledge gap. Within the project, microtopography and groundwater table information has been successfully mapped for the study sites. Biomass has not yet been mapped and the work in this thesis will be used for this purpose.

Prior to mapping biomass on a regional scale, local field-based estimates are required. Field-based biomass estimates are used to calibrate and validate regional estimates. Allometric equations are typically used for this purpose, however, very few equations exist for peatland shrub species. For this reason, we developed our own allometric equations. The process of developing these equations is presented in Chapter 2, and is designed to provide insight on some heavily discussed topics in the allometric literature. Topics include whether the allometry in peatland shrubs are different from wetland shrubs and whether a generalized equation can be used in replacement of genus-specific equations.

The regional estimates of biomass will be obtained through UAV-collected data. Previous biomass estimation studies, using UAVs, have demonstrated their capabilities in capturing low stature shrubs. Through this platform, structural and spectral parameters can be examined to determine the best predictor of aboveground biomass. We will also be able to assess the accuracy of UAV-derived biomass estimates compared to the field data. This study is presented in Chapter 3.

1.4 Research Objectives

Two main objectives are addressed in this research:

1.To develop allometric equations for dominant shrub species found in a boreal continental fen.

a. Assess the portability of previously published allometric equations for the same shrub species.
b. Assess the need for genus-specific equations

2.To assess the capacity of UAV photogrammetry for mapping aboveground biomass in a boreal continental fen.

a. Compare the relative value of spectral and structural variables for measuring shrubby AGB
b. Create an AGB map of shrub biomass of the study area using the best predictor variable.

1.5 Organization of thesis

Two independent research articles were written to satisfy each independent research objective. The same study site was used for the analysis of both objectives. Chapter 2 explains the development of the allometric models and addresses common debates in the allometric literature. Chapter 3 accounts reports the accuracy of using UAVs to estimate and map aboveground biomass. Chapter 4 summarizes the major conclusions drawn from Chapter 2 and Chapter 3 and details limitations with the research and also outlines potential opportunities for future research.

Chapter Two: Developing Allometric Equations for Estimating Shrub Biomass in a Boreal Fen

2.1 Abstract

Allometric equations for estimating aboveground biomass (AGB) from easily measured plant attributes are unavailable for most species common to mid-continental boreal peatlands, where shrubs comprise a large component of the vegetation community. Our study develops allometric equations for three dominant genera found in boreal fens: *Alnus* spp. (alder) *Salix* spp. (willow), and *Betula pumila* (bog birch). Two different types of local equations were developed: (1) individual equations based on genus/phylogeny, and (2) a general equation that pooled all individuals regardless of genera. The general equation had a R^2 = 0.97 (n = 82) and was not significantly different (p > 0.05) than any of the phylogenetic equations. This indicated that a single generalized equation is sufficient in estimating AGB for all three genera occurring in our study area. A closer look at the performance of the general equation revealed that smaller stems were predicted less accurately than larger stems because of the higher variability of leafy biomass found in small individuals. Previously published equations developed in other ecoregions did not perform as well as our local equations.

2.2 Introduction

We require improved strategies for quantifying vegetation biomass in peatlands (Brown, 2002; Nwaishi et al., 2015) which contain mostly non-merchantable plant species that tend to be under-represented in the literature. Peatlands—a type of wetland that accumulates organic matter—store approximately one third of the planet's soil carbon (Tarnocai, 2009) while comprising just 3% of the total land surface (Yu et al., 2010). Since plants facilitate carbon storage through photosynthesis (Le Quere et al., 2017), vegetation-biomass estimates are necessary for calculating carbon budgets (Le Toan et al., 2011; Paul et al., 2016) and are a key element of carbon-dynamics models (Zhang et al., 2002). Ground-based measurements of standing biomass are also useful for calibrating and validating remote-sensing models (e.g., Lefsky et al 1999 and Kankare et al 2013) and can provide valuable information on wildlife habitat (Hyde et al., 2006), fire behavior (Keeley, 2009), and biofuel stock (Stasko et al., 2011) .

Direct measurement of vegetation biomass is expensive and time-consuming (Verwijst & Telenius,1999) and allometric equations provide efficient alternatives to destructive sampling (Seidel et al., 2011). Allometry uses one or more plant dimensions (e.g., tree diameter at breast height) to estimate a separate dimension (e.g., stem volume) that is more difficult to obtain. However, most published allometrics focus on commercially valuable tree species (e.g. TerMikaelian & Korzukhin, 1997 and Zianis & Mencuccini, 2004). This is especially problematic for researchers working in boreal peatlands, where trees comprise a relatively small proportion of vegetation communities (Whitehouse & Bayley, 2005).

Shrubs are multi-stemmed woody plants that can account for up to 88% of the total aboveground biomass in Canadian continental boreal peatlands, based on the synthesis done in Campbell et al. (2000). However, the literature on peatland-shrub allometry is scant. Connolly and Grigal (1983) provide one of the few-known sources of allometric equations for wetland shrubs, but the portability of these—or other models from mixed or upland areas—to boreal peatlands remains unassessed. Here, we define *portability* as the ability of an allometric equation to perform effectively under conditions that are different from those where it was originally developed. Previous research has shown that species can produce strong effects on allometric relationships (Mosseler et al., 2016). Similarly, allometric equations can vary substantially from one region to another (Law et al., 2001; Muukkonen, 2007; Paul et al., 2016). Buech and Rugg (1989) inspected biomass-allometry relations for five species of shrubs common to northeastern Minnesota and found that species- and site-specific equations were more effective than generalized equations, with few exceptions. The value of local equations for shrub-biomass estimation has been reported in the western Himalaya (Mandal & Joshi, 2015), Argentina (Rojo et al., 2017), and northeastern California (Huff et al., 2017). However, this finding is not universal. For example, Berner et al. (2015) found that allometric relationships for dwarf birch (*Betula nana* L.) varied little across forest and tundra ecosystems in Siberia and Alaska. Other authors (Paul et al., 2013; Roxburgh et al., 2015; Sun et al., 2017) have emphasized the controls of plant size on allometrics, highlighting the importance of remaining within the size domain of the equations. Portability of equations is important in allometric studies because an equation that can be used across multiple regions can greatly reduce the amount of time, labor, and destructive sampling involved with biomass estimation.

The overall objective of the research reported in this paper was to develop effective allometric equations for estimating aboveground shrub biomass at a boreal fen in west-central Alberta, Canada. In doing so, we first assessed the portability of published allometric equations for shrubs (Connolly & Grigal, 1983; Brand & Smith, 1985; Berner et al., 2015) to our study area, and then assessed the need for genus-specific equations, which we refer to as *phylogenetic equations* in this paper.

2.3 Methodology

2.3.1 Study Area

Field work was conducted at two sites near the Canadian town of Peace River, Alberta, in the northern boreal region of the province (Figure 2.1 & Figure 2.2). Both sites fall within the Dry Mixedwood natural subregion, where the mean annual temperature is 1 °C and mean annual precipitation is 461 mm (Natural Regions Committee, 2006). This subregion's climate is characterized by warmer summers and milder winters compared to the other subregions in the boreal forest region (Natural Regions Committee, 2006). Site 1 is a shrubby fen composed primarily of alder (A*lnus* spp.), willow (*Salix* spp.), and bog birch (*Betula pumila* L.) ranging in height from 30 cm to 4 m. Site 2 is also a shrubby fen hosting the same primary species as Site 1 with the addition of paper birch (*Betula papyrifera* Marshall). The vegetation on Site 2 ranged up to 9 m in height and was added primarily to include samples at the top end of the height range (>2 m).

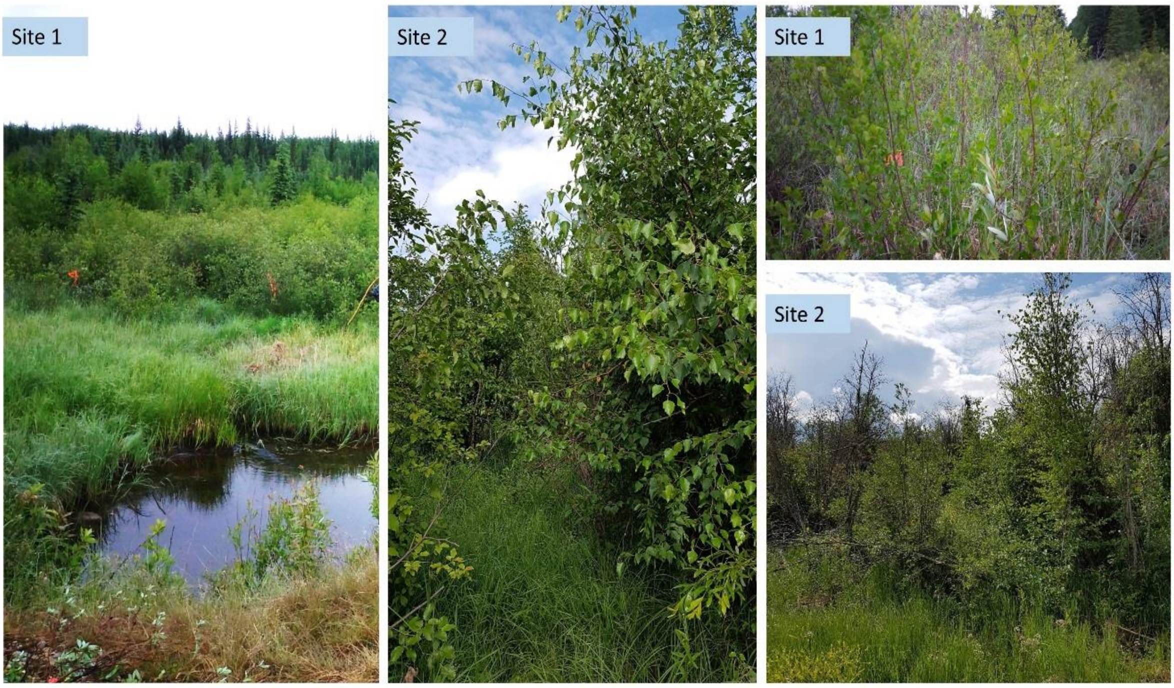

Figure 2.1: *Field photos of Site 1 and Site 2. The photos for Site 1 were taken during June 2017; those for Site 2 were taken in April 2016.*

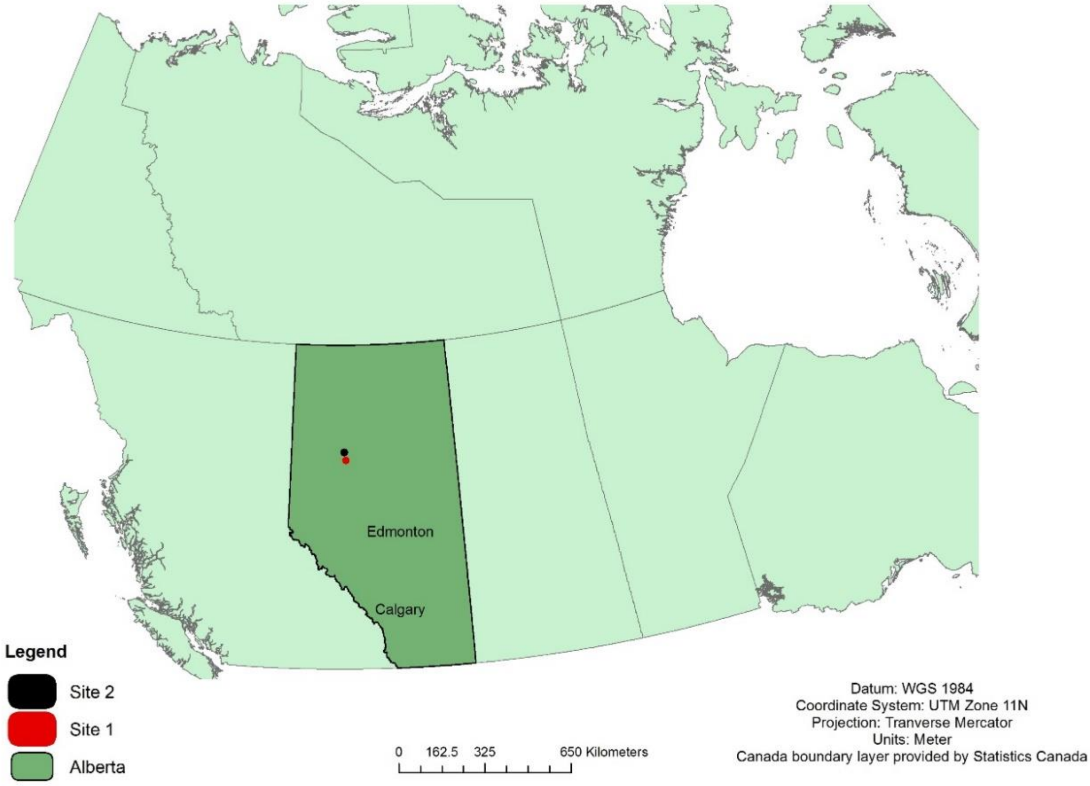

Figure 2.2: *Map of Canada showing the location of Study Site 1 (56.9˚ N latitude, 116.8˚ W longitude) and Study Site 2 (56.4˚ N latitude, 116.8˚ W longitude).*

2.3.2 Aboveground Biomass Sampling

We first visited the study area on 5 June 2017 to perform a preliminary survey which gathered information on the range of sizes for each shrub genus across Site 1. During this survey, four transects were delineated to run east-west across the site and spaced 25 m apart. Every 10 m along the transect, the height of all shrubs that fell within ~0.5 m radius of the point was recorded. The locations of these plants were recorded on a Garmin Montana 600 handheld GPS and the shrubs were marked with flagging tape. All marked plants were then categorized by their height and genus. A stratified random sampling approach was used to choose the shrubs that would be harvested in a second visit, to ensure that the destructively sampled shrubs would be representative of the size variability within each genus.

Site 2 was added to the study to incorporate larger individuals (>2 m in height) for the development of allometric equations. A field survey for a separate project indicated that the shrubs found on Site 2 were larger than the ones that are found on Site 1. The inclusion of these larger individuals allowed for the developed equations to be applicable to a wider range of heights.

Destructive sampling on Site 1 took place on 15 June 2017; sampling on Site 2 was completed on 21 August 2017. A total of 55 shrubs were harvested. The number of stems for each shrub ranged from 1–30 (Table 2.1). Three stems from each individual shrub were chosen to be included in the development of allometric equations, resulting in approximately thirty stems per genus from Site 1. Only one stem per shrub was harvested for samples collected from Site 2 (Table 2.1). Field crews cut stems as close to the ground as possible and stored them at 4 °C for no longer than 48 h prior to processing. Stem length, basal diameter, and stem diameter at 15 cm height were measured in the laboratory. Stem length (to the nearest centimeter) was measured with a standard measuring tape, and basal diameter (to the nearest 0.1 millimeter) was measured using a digital caliper. Samples were then dried at 70 °C until a constant mass was reached. The leaves and stems were separated and weighed with a Denver Instrument SI-6002 scale that measured to the nearest gram. The descriptive statistics for all destructive samples can be found in Table 2.1.

Table 2.1: *Descriptive statistics of shrubs harvested at each of the two study sites.*

	Shrubs Harvested	**Stems Harvested**	**Average Height (m)**	**Average Number of Stems per Shrub**	**Basal Diameter Range (cm)**	**Stem Length Range (cm)**	**Dried Stem Biomass Range (g)**
Site 1							
Alnus spp.	8	21	3.09	8	0.64–5.70	89–389	16–1598
Salix spp.	16	37	1.46	26	0.31–2.76	60–209	7–386
Betula pumila	13	25	1.59	18	0.31–1.37	39–250	6–129
Site 2							
Alnus spp.	6	6	4.89	1	3.12–5.18	381–545	643–2718
Salix spp.	12	12	3.45	1	1.16–2.75	242–450	78–1635

2.3.3 Allometrics

2.3.3.1 Local Equations

We developed local allometric equations for aboveground dry biomass (*M)* as:

$$M = aD^b, \tag{1}$$

Where a and b are the fitted coefficients and D is the basal diameter. IBM SPSS 24.0 (IBM Corporation, Armonk, NY, USA) statistical software was used for the development of all equations. We elected to use non-linear models, which assume normally distributed and additive errors, over log-transformed linear models, which assume log-normally distributed and multiplicative errors, for two reasons. First, the few existing allometric models for wetland shrubs (Connolly & Grigal, 1983; Brand & Smith, 1985; Berner et al., 2015) are also non-linear. Developing similar models provided an easier means of comparing parameters and fulfilling our first objective. The power-function form of the model used here has been employed by many previous researchers (e.g. Bond-Lamberty & Wang, 2002, Paul et al. 2013 and Berner et al. 2015). Second, our project goals included developing models of stand biomass, and non-linear models do a better job with larger individuals. We tested both basal diameter and stem length as the measurable parameter but achieved better results with basal diameter, as have others (Roussopoulos & Loomis, 1979; Connolly & Grigal, 1983; Brand & Smith, 1985; TerMikaelian & Korzukhin, 1997; Brown, 2002; Paul et al., 2016). We worked here in the frequentist framework. No Bayesian prior probabilities were employed.

Recognizing the lack of independence in our samples from collecting multiple stems from one shrub, we also used a mixed-model approach, with the basal diameter as the fixed effect and the individual shrub as the random effect. We found that the mixed model was not statistically different from the ordinary least squares (OLS) regression model, so we continued with the OLS approach for reasons of parsimony.

Two categories of equations were developed for predicting aboveground biomass: (i) a general equation, and (ii) phylogenetic equations based on genera. The general equation drew from all available shrubs sampled at our study sites, regardless of size or genera. We did, however, randomly reduce the number of contributing *Salix* samples for the general equation from 49 to 30 in order to avoid overrepresentation of *Salix* compared to other shrub genera. Phylogenetic equations were developed for each of the three shrub genera present at our study sites: *Alnus*, *Salix*, and *Betula.* The accuracy and goodness-of-fit for each equation were assessed using standard root-mean-square errors (RMSE) and coefficients of determination (R^2) metrics. We tested for significant differences amongst equation coefficients using *t*-tests, where *t* values were calculated as:

$$t = \frac{b_1 - b_2}{\sqrt{SEb_1^2 - SEb_2^2}} \tag{2}$$

where b_1 is the coefficient of equation 1 and b_2 is the coefficient of equation 2; SEb_1 and SEb_2 are the standard error of each equation coefficient, respectively. The null hypothesis is that there is no difference between the coefficients being compared. The purpose of this test is to determine if the rate of change between basal diameter and aboveground biomass is different across the equations. Therefore, the slope coefficient was first tested using this test. If there were no significant differences between the slope coefficients, the test statistic described by Zar (1999) was used to compare the *a* coefficient (or *y*-intercept).

2.3.3.2 Published Equations

Published phylogenetic equations that were reported as a power function and that used basal diameter as the measurable parameter were compared against our general equation. Berner et al. (2015) and Connolly & Grigal (1983) developed phylogenetic equations for the same three genera across arctic sites and wetland sites, respectively. Brand & Smith (1985) developed an equation for *Salix* spp. compiled from three other sources whose study sites were in Minnesota. The R^2 and RMSE for each published regression was calculated against the samples from our study. The slope coefficient was also compared against the slope coefficient for the general equation (Equation (2)).

2.4 Results

2.4.1 Local Equations

Table 2.2 summarizes the equation parameters, accuracy, and goodness-of-fit for each of the 5 local equations developed for our study area. All phylogenetic equations had an R^2 > 0.9, corroborating that basal diameter is a significant predictor of aboveground biomass. The high R^2 value of the general equation (R^2 = 0.967, RMSE = 0.293 grams) suggests that it can be used to accurately estimate the biomass of all three phylogenetic groups. There was no significant difference between the coefficients of the general equation with any of the phylogenetic equations ($p > 0.05$), suggesting that such differentiation is not necessary at our study site.

Table 2.2: *Summary of the allometric equations relating basal diameter to aboveground biomass, including coefficients of determination (R^2), mean absolute percentage error (MAPE), root-mean-square errors (RMSE), and cross validated RMSE (CV-RMSE). The reported n represents number of stems. A 10-fold cross validation was repeated 10 times to obtain the CV-RMSE. The sample size (n) is the number of stems used to develop each regression. T-values represent differences in y-intercept (a) and slope (b) from that of the general equation, and include p-values. Those differences that are significant at the 0.05 threshold are marked as *.*

	n	***a***	***B***	R^2	**RMSE(g)**	**MAPE**	**CV-RMSE(g)**	***a* Test-*t*-Value (*p*)**	***b* Test-*t*-Value (*p*)**
Phylogenetic Equations									
Alnus	27	44.06	2.395	0.983	0.209	2.9%	0.194	1.83 (0.07)	1.83 (0.07)
Salix	49	55.85	2.325	0.943	0.344	6.2%	0.325	0.94 (0.35)	1.56 (0.12)
Betula	25	49.52	2.027	0.907	0.254	7.2%	0.260	0.19 (0.85)	0.77 (0.44)
Alnus & Salix	76	52.88	2.291	0.961	0.314	5.4%	0.293	0.44 (0.66)	0.56 (0.57)
General Equation									
General	82	53.37	2.251	0.967	0.291	5.9%	0.287	N/A	N/A

2.4.2 Published Equations

Table 2.3 summarizes the parameters of the published equations found in the literature. The Conolly & Grigal (1983) equations (R^2 = 0.879–0.956) predicted biomass at our sites better than the Berner et al. equations (R^2 = 0.608–0.810). The *Salix* equation from Brand & Smith (1985) also had a high goodness of fit (R^2 = 0.947). When compared to our general equation, however, all equations were significantly different, with the exception of the *Salix* equation published by Conolly & Grigal (1983). There were also significant differences between the published equations and each phylogenetic equation. We could not test for differences in the *a* coefficient because we did not have access to the data used to develop the published equations.

Table 2.3: *Summary of the published allometric equations relating basal diameter to aboveground biomass. The reported coefficients of determination (R^2) and root-mean-square errors (RMSE) were calculated in relation to the local data in estimating aboveground biomass. D Range is the basal diameter range for stems used for the development of each equation. T values represent differences in slope (b) from that of the general equation, and include p-values. Those differences that are significant at the 0.05 threshold are marked as *.*

	D Range **(cm)**	***a***	***b***	R^2	**RMSE (g)**	***b Test-*** ***t*-Value (*p*)**
Conolly & Grigal (1983)						
Alnus rugosa	0.25–3	33.722	2.712	0.880	0.558	4.56 (<0.01) *
Salix spp.	0.25–3	60.153	2.202	0.962	0.315	0.72 (0.48)
Betula pumila	0.25–2.25	59.777	2.579	0.930	0.426	3.92 (<0.01) *
Berner et al. (2015)						
Alnus spp. pooled	0.18–9.52	19.40	2.78	0.608	1.006	3.18 (<0.01) *
Salix spp. pooled	0.01–6.30	21.80	2.64	0.687	0.899	2.64 (<0.01) *
Betula spp. pooled	0.09–2.53	28.97	2.88	0.810	0.701	5.28 (<0.01) *
Brand & Smith (1985)						
Salix spp.	0.25–3.81	44.86	2.539	0.947	0.372	3.81 (<0.01) *

2.5 Discussion

2.5.1 The value of phylogenetic equations

Our testing indicated that the relationship between basal diameter and aboveground biomass did not differ significantly across genera, and that there was no significant difference between phylogenetic equations and the general equation developed for our study area. These findings are similar to Sun et al. (2017), who found phylogeny to exert little influence on allometric coefficients for shrubs in China. In our study area, the physical differences were most apparent between *Alnus* and *Betula*. *Alnus* individuals, in comparison with the other two genera, had a more tree-like appearance, were generally larger and had a lower number of stems, whereas *Betula* individuals were much smaller and many-stemmed (Table 2.1). The growth form of *Salix* was more variable than the other two genera; some individuals more closely resembled *Alnus* whereas others resembled *Betula*. Looking deeper among the phylogenetic equations (Table 2.4), we found *Betula* equations to be significantly different from *Alnus* (p = 0.02) and marginally different from *Salix* (p = 0.07). *Alnus* and *Salix* equations were very similar (p = 0.50). As a follow-up, we combined *Alnus* and *Salix* samples to test if the removal of *Betula* would create a significant change in the general equation. This modified equation was found to be not significantly different from the general equation (Table 2.2) and was also not significantly different from the *Betula* equation (p = 0.08). Despite the physical differences in *Betula* compared to the other two genera, the inclusion of these samples did not significantly change the general equation.

Table 2.4: *Comparison of local phylogenetic equations. T values represent differences in slope (b) from that of the general equation and include p-values. Those differences that are significant at the 0.05 threshold are marked as *.*

	Alnus	***Betula***	***Salix***	***Alnus-Salix***
Alnus	-	-	-	-
Betula	2.45 (0.02) *	-	-	-
Salix	0.67 (0.50)	1.86 (0.07)	-	-
Alnus-Salix	1.25 (0.22)	1.80 (0.08)	0.34 (0.73)	-

2.5.2 Equation Portability

A comparison of previously published equations with our local equations showed that we were unable to apply external equations to our study site. The Conolly & Grigal (1983) and Brand & Smith (1985) equations, with the exception of one, were significantly different from our general equation (Table 2.3). The Berner et al. (2015) equation had a relatively lower R^2 and higher RMSE compared to the other two publications (Table 2.3). The Berner et al. (2015) equation was developed across arctic sites which may explain the lower goodness of fit. A common conclusion about equation portability is that it is more accurate when the sample size is larger and includes samples across many different sites (Levia, 2008; Shaiek et al., 2011; Forrester et al., 2017). Our study has a relatively small number of samples and study sites compared to the other three allometric studies. These limitations could reduce the portability of our equation to other regions, however, given the lack of wetland shrub specific allometric equations, equations presented here represent an important step to improved estimation of biomass across boreal peatlands.

2.5.3 The Variability in Size Classes

Some allometric studies have found success in the use of size-based equations instead of phylogenetic equations. For example, Paul et al. (2016) generalized equations from species to plant functional types and noticed a minimal loss of accuracy. They found that the key differences in allometry are between trees, tall shrubs, and short shrubs which they attributed to the differences in stem geometry, life-span, woody density, and environmental conditions. We examined how size may influence the accuracy of our general equation by calculating the mean absolute percentage error (MAPE) for three categories of basal diameter class: (i) <1 cm, (ii) 1–2 cm, and (iii) >2 cm. The results are found in Table 2.5. MAPE is highest for the <1 cm class (8.2%) and lowest for the >2 cm class (2.0%). These results suggest that less of the variability found in the smaller shrubs (<1 cm class) is accounted for by the general equation. Figure 2.3 displays the general equation plotted alongside a regression line fit to each size class. The R^2 and RMSE values (Figure 2.3) report the goodness of fit of the general equation with the points used to develop each size-based regression line. The R^2 value was the highest for >2 cm basal diameter class (R^2 = 0.88) and lowest for <1 cm basal diameter class (R^2 = 0.65). The slope coefficients for each size-based regression line was tested against the slope of the generation equation using Equation (2). We found that there were significant differences between the general equation and those based on shrub size; particularly in the <1 cm (p < 0.01) and 1–2 cm (p = 0.05) basal diameter classes (Table 2.5). There was no significant difference between the general equation and the >2 cm basal diameter class (p = 0.72).

Table 2.5: *The mean average percentage error is reported for each group of samples separated by basal diameter size. T-values represent differences in slope (b) from that of the general equation and include p-values. Those differences that are significant at the 0.05 threshold are marked as *.*

	<1 cm Class	**1–2 cm Class**	**>2 cm Class**
MAPE	8.2%	5.3%	2.0%
t-value	4.58 (<0.01) *	2.00 (0.05) *	0.36 (0.72)

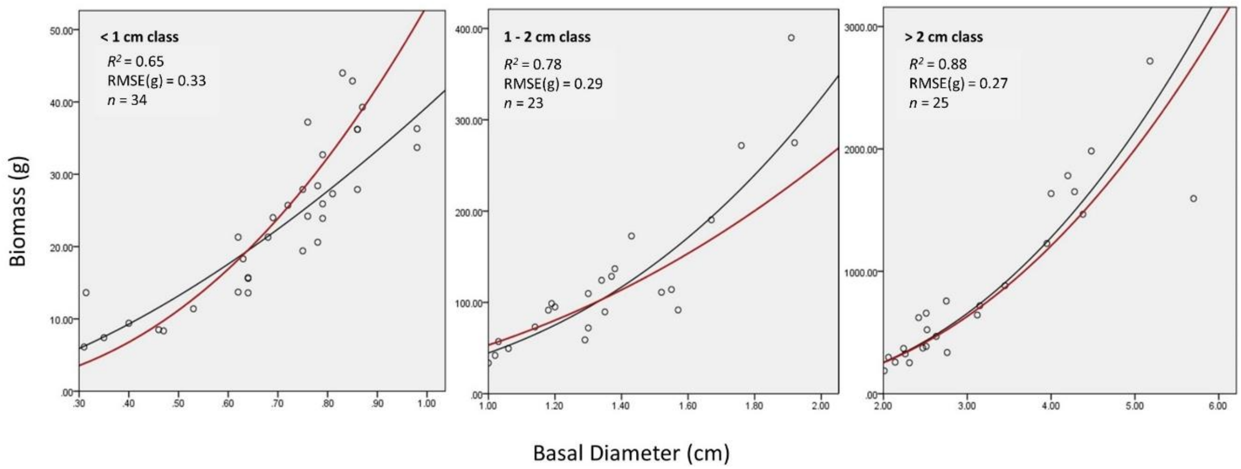

Figure 2.3: *All samples separated into three basal diameter classes. The black line is a regression line that was fit for each group of samples. R^2 and RMSE are reported based on how well the red line, the general regression line, fits each group of samples.*

In order to further explore internal patterns in this dataset, we calculated the proportion of leafy biomass (B_l) as:

$$B_l = \frac{Leaf\ Biomass}{Total\ Biomass} \times 100 \qquad (3)$$

for each individual. Box plots displaying B_l for each basal-diameter class are shown in Figure 2.4. We found both a higher mean proportion (22.4% for <1 cm basal diameter) and range (9.1% to 41.2%) of leafy biomass for small basal-diameter individuals than medium (15.9% mean and 4.9% to 30.5% range for 1–2 cm basal diameter) and large (13.2% mean and 2.9% to 25.0% range for >2 cm basal diameter) individuals. Other studies have found a decline in leafy mass and an increase in stem mass as a tree ages (Porte et al., 2000; Wutzler et al., 2008; Shaiek et al., 2011). Forrester et al. (2017) also noticed that foliage mass is more variable than stem or aboveground biomass. Based on these studies, we theorize that the increased leafy biomass variability found in the <1 cm basal diameter class may contribute to the poorer fit of the general allometric equation for this class; however, more data is required to confirm this observation.

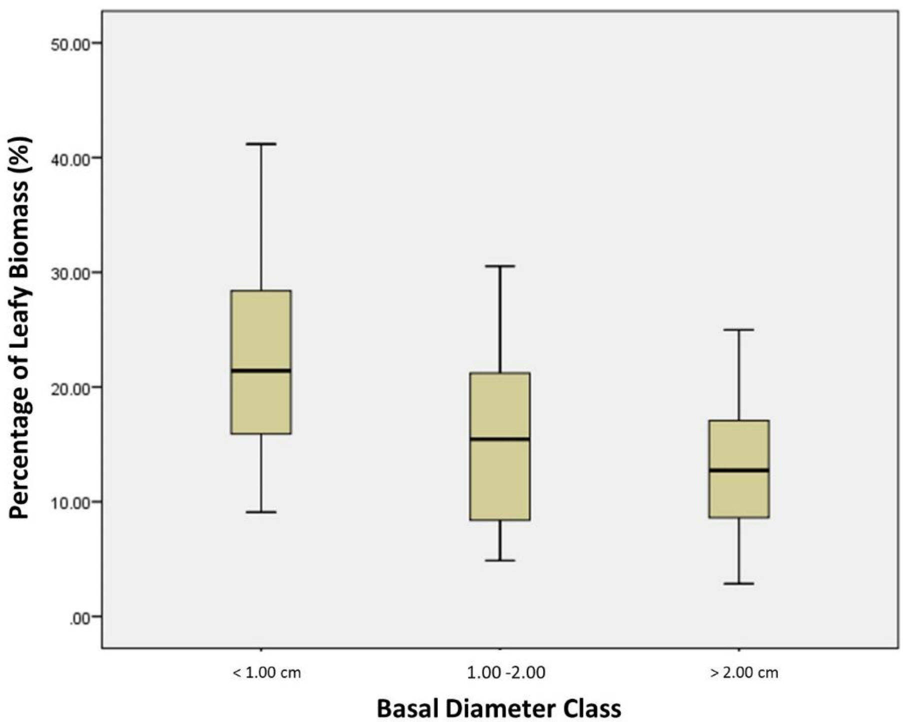

Figure 2.4: *Box plots of the percentage of the total biomass that is represented by the leafy biomass for each basal diameter class.*

2.6 Conclusions

Allometric equations developed for shrubs have been underrepresented in the literature. Our study has developed three phylogenetic equations and one general equation that accurately estimated the aboveground biomass (AGB) in a boreal fen. Important lessons were learned which addressed some of the highly debated topics found in the allometric literature (Buech & Rugg., 1989; Law et al., 2001; Muukkonen, 2007; Berner et al., 2015; Mandal & Joshi., 2015; Paul et al., 2016; Rojo et al., 2017; Huff et al., 2017). We found that local equations provide more accurate

AGB estimates compared to previously published equations developed in other ecoregions (Table 2.3). We also found that equations based on shrub genus were not significantly different from a pooled equation of all shrub genera (Table 2.2). Through our analysis, we noticed a higher variability in the proportion of leafy biomass for smaller shrubs (<1 cm basal diameter) compared to larger shrubs (>1 cm basal diameter) (Figure 2.4). This higher variability may explain why the AGB of smaller shrubs were predicted less accurately. If this is the case, future allometric studies may consider excluding leafy biomass to avoid the increased variability.

Although the portability of our local equations remains unassessed, these boreal-peatland specific equations can be used as a baseline for testing in other peatland sites. These equations will also be useful for future efforts in estimating biomass in boreal peatland regions.

2.7 References

Berner, L. T., Alexander, H. D., Loranty, M. M., Ganzlin, P., Mack, M. C., Davydov, S. P., & Goetz, S. J. (2015). Biomass allometry for alder, dwarf birch, and willow in boreal forest and tundra ecosystems of far northeastern Siberia and north-central Alaska. *Forest Ecology and Management*, *337*, 110-118.

Bond-Lamberty, B., Wang, C., & Gower, S. T. (2002). Aboveground and belowground biomass and sapwood area allometric equations for six boreal tree species of northern Manitoba. *Canadian Journal of Forest Research*, *32*(8), 1441-1450.

Brand, G. J., & Smith, W. B. (1985). Evaluating allometric shrub biomass equations fit to generated data. *Canadian Journal of Botany*, *63*(1), 64-67.

Brown, S. (2002). Measuring carbon in forests: current status and future challenges. *Environmental pollution*, *116*(3), 363-372.

Buech, R. R., & Rugg, D. J. (1989). Biomass relations of shrub components and their generality. *Forest Ecology and Management*, *26*(4), 257-264.

Campbell, C., Vitt, D. H., Halsey, L. A., Campbell, I. D., Thormann, M. N., & Bayley, S. E. (2000). Net primary production and standing biomass in northern continental wetlands. *Information Report-Northern Forestry Centre, Canadian Forest Service,* (NOR-X-369).

Connolly, B. J., & Grigal, D. F. (1983). Biomass estimation equations for wetland tall shrubs.

Forrester, D. I., Tachauer, I. H. H., Annighoefer, P., Barbeito, I., Pretzsch, H., Ruiz-Peinado, R., ... & Saha, S. (2017). Generalized biomass and leaf area allometric equations for European tree species incorporating stand structure, tree age and climate. *Forest ecology and management*, *396*, 160-175.

Huff, S., Ritchie, M., & Temesgen, H. (2017). Allometric equations for estimating aboveground biomass for common shrubs in northeastern California. *Forest ecology and management*, *398*, 48-63.

Hyde, P., Dubayah, R., Walker, W., Blair, J. B., Hofton, M., & Hunsaker, C. (2006). Mapping forest structure for wildlife habitat analysis using multi-sensor (LiDAR, SAR/InSAR, ETM+, Quickbird) synergy. *Remote Sensing of Environment*, *102*(1-2), 63-73.

Kankare, V., Räty, M., Yu, X., Holopainen, M., Vastaranta, M., Kantola, T., ... & Viitala, R. (2013). Single tree biomass modelling using airborne laser scanning. *ISPRS journal of photogrammetry and remote sensing*, *85*, 66-73.

Keeley, J. E. (2009). Fire intensity, fire severity and burn severity: a brief review and suggested usage. *International Journal of Wildland Fire*, *18*(1), 116-126.

Law, B. E., Van Tuyl, S., Cescatti, A., & Baldocchi, D. D. (2001). Estimation of leaf area index in open-canopy ponderosa pine forests at different successional stages and management regimes in Oregon. *Agricultural and Forest Meteorology*, *108*(1), 1-14.

Le Quéré, C., Andrew, R. M., Friedlingstein, P., Sitch, S., Pongratz, J., Manning, A. C., ... & Boden, T. A. (2017). Global carbon budget 2017. *Earth System Science Data Discussions*, 1-79.

Le Toan, T., Quegan, S., Davidson, M. W. J., Balzter, H., Paillou, P., Papathanassiou, K., ... & Ulander, L. (2011). The BIOMASS mission: Mapping global forest biomass to better understand the terrestrial carbon cycle. *Remote sensing of environment*, *115*(11), 2850-2860.

Lefsky, M. A., Harding, D., Cohen, W. B., Parker, G., & Shugart, H. H. (1999). Surface lidar remote sensing of basal area and biomass in deciduous forests of eastern Maryland, USA. *Remote sensing of Environment*, *67*(1), 83-98.

Levia Jr, D. F. (2008). A generalized allometric equation to predict foliar dry weight on the basis of trunk diameter for eastern white pine (Pinus strobus L.). *Forest ecology and management*, *255*(5-6), 1789-1792.

Mandal, G., & Joshi, S. P. (2015). Estimation of above-ground biomass and carbon stock of an invasive woody shrub in the subtropical deciduous forests of Doon Valley, western Himalaya, India. *Journal of Forestry Research*, *26*(2), 291-305.

Mosseler, A., Major, J. E., & Larocque, G. R. (2016). Allometric relationships from coppice structure of seven North American willow (Salix) species. *Biomass and Bioenergy*, *88*, 97-105.

Muukkonen, P. (2007). Generalized allometric volume and biomass equations for some tree species in Europe. *European Journal of Forest Research*, *126*(2), 157-166.

Natural Regions Committee. (2006). Natural regions and subregions of Alberta. *Government of Alberta*

Nwaishi, F., Petrone, R. M., Price, J. S., & Andersen, R. (2015). Towards developing a functional-based approach for constructed peatlands evaluation in the Alberta Oil Sands Region, Canada. *Wetlands*, *35*(2), 211-225.

Paul, K. I., Roxburgh, S. H., Chave, J., England, J. R., Zerihun, A., Specht, A., ... & Huxtable, D. (2016). Testing the generality of above-ground biomass allometry across plant functional types at the continent scale. *Global change biology*, *22*(6), 2106-2124.

Paul, K. I., Roxburgh, S. H., England, J. R., Ritson, P., Hobbs, T., Brooksbank, K., ... & Neumann, C. (2013). Development and testing of allometric equations for estimating above-ground biomass of mixed-species environmental plantings. *Forest Ecology and Management*, *310*, 483-494.

Porté, A., Bosc, A., Champion, I., & Loustau, D. (2000). Estimating the foliage area of Maritime pine (Pinus pinaster Aït.) branches and crowns with application to modelling the foliage area distribution in the crown. *Annals of Forest Science*, *57*(1), 73-86.

Rojo, V., Arzamendia, Y., Pérez, C., Baldo, J., & Vilá, B. (2017). Double Sampling Methods in Biomass Estimates of Andean Shrubs and Tussocks. *Rangeland Ecology & Management*, *70*(6), 718-722.

Roussopoulos, P. J., & Loomis, R. M. (1979). Weights and dimensional properties of shrubs and small trees of the Great Lakes conifer forest. *Research Paper NC-178. St. Paul, MN: US Dept. of Agriculture, Forest Service, North Central Forest Experiment Station, 178*.

Roxburgh, S. H., Paul, K. I., Clifford, D., England, J. R., & Raison, R. J. (2015). Guidelines for constructing allometric models for the prediction of woody biomass: how many individuals to harvest?. *Ecosphere*, *6*(3), 1-27.

Seidel, D., Fleck, S., Leuschner, C., & Hammett, T. (2011). Review of ground-based methods to measure the distribution of biomass in forest canopies. *Annals of Forest Science*, *68*(2), 225-244.

Shaiek, O., Loustau, D., Trichet, P., Meredieu, C., Bachtobji, B., Garchi, S., & Aouni, M. H. E. (2011). Generalized biomass equations for the main aboveground biomass components of maritime pine across contrasting environments. *Annals of forest science*, *68*(3), 443.

Stasko, T. H., Conrado, R. J., Wankerl, A., Labatut, R., Tasseff, R., Mannion, J. T., ... & Knott, G. (2011). Mapping woody-biomass supply costs using forest inventory and competing industry data. *biomass and bioenergy*, *35*(1), 263-271.

Sun, H., Wang, X., Fan, Y., Liu, C., Wu, P., Li, Q., & Yin, W. (2017). Effects of biophysical constraints, climate and phylogeny on forest shrub allometries along an altitudinal gradient in Northeast China. *Scientific Reports*, *7*, 43769.

Tarnocai, C. (2009). The impact of climate change on Canadian peatlands. *Canadian Water Resources Journal*, *34*(4), 453-466.

Ter-Mikaelian, M. T., & Korzukhin, M. D. (1997). Biomass equations for sixty-five North American tree species. *Forest Ecology and Management*, *97*(1), 1-24.

Verwijst, T., & Telenius, B. (1999). Biomass estimation procedures in short rotation forestry. *Forest Ecology and Management*, *121*(1-2), 137-146.

Whitehouse, H. E., & Bayley, S. E. (2005). Vegetation patterns and biodiversity of peatland plant communities surrounding mid-boreal wetland ponds in Alberta, Canada. *Canadian Journal of Botany*, *83*(6), 621-637.

Wutzler, T., Wirth, C., & Schumacher, J. (2008). Generic biomass functions for Common beech (Fagus sylvatica) in Central Europe: predictions and components of uncertainty. *Canadian Journal of Forest Research*, *38*(6), 1661-1675.

Yu, Z., Loisel, J., Brosseau, D. P., Beilman, D. W., & Hunt, S. J. (2010). Global peatland dynamics since the Last Glacial Maximum. *Geophysical Research Letters*, *37*(13).

Zar, J.H. (1999) *Biostatistical Analysis,* 4th ed.; Prentice Hall: Upper Saddle River, NJ, USA pp. 324–359.

Zhang, Y., Li, C., Trettin, C. C., Li, H., & Sun, G. (2002). An integrated model of soil, hydrology, and vegetation for carbon dynamics in wetland ecosystems. *Global Biogeochemical Cycles*, *16*(4), 9-1.

Zianis, D., & Mencuccini, M. (2004). On simplifying allometric analyses of forest biomass. *Forest Ecology and Management*, *187*(2-3), 311-332.

2.8 Erratum

This erratum outlines the changes that have been made to Chapter 2 based on feedback from the examining committee at the defense examination.

i. Equation (2) (found on p. 28) is a t-test that was used to compare the coefficients from the phylogenetic equation with those of the general equation. The results from this test were used to conclude that the general equation was not significantly different from each individual phylogenetic equation. We acknowledge that this test was not appropriately used because the samples used to develop each phylogenetic equation were the same samples used to develop the general equation. Therefore, we are not comparing two independent regression lines. To overcome this issue, a generalized linear model (GLM) was used to test genus type as a predictor variable. The GLM was processed in RStudio and we found that genus information was a not a significant predictor of AGB ($p > 0.05$) (Table 2.6). The conclusions made from this analysis are consistent with those made from the t-test. Therefore, no changes were required.

Table 2.6: *Output values from the generalized linear model analysis executed in R statistical software.*

Basal Diameter	Standard Error	Z-value	P-value
Basal Diameter	0.34	3.394	< 0.01
Genus - Willow	0.20	0.345	0.73
Genus – Bog Birch	0.27	0.116	0.91
Genus – Alder	0.23	0.215	0.83

ii. Table 2.5 and Figure 2.3 were used to demonstrate the variability found across size classes. The examiners believed a residual plot would be better used in observing variability across basal diameters. Figure 2.5 shows the mean average percentage error (MAPE) for each associated basal diameter. It appears that when basal diameter is less than 1 cm, there is a higher variability in MAPE whereas when basal diameter is larger than 2 cm, the MAPE remains consistently below 10%. These results were consistent with those found in Table 2.5 and Figure 2.3, therefore, no changes were required.

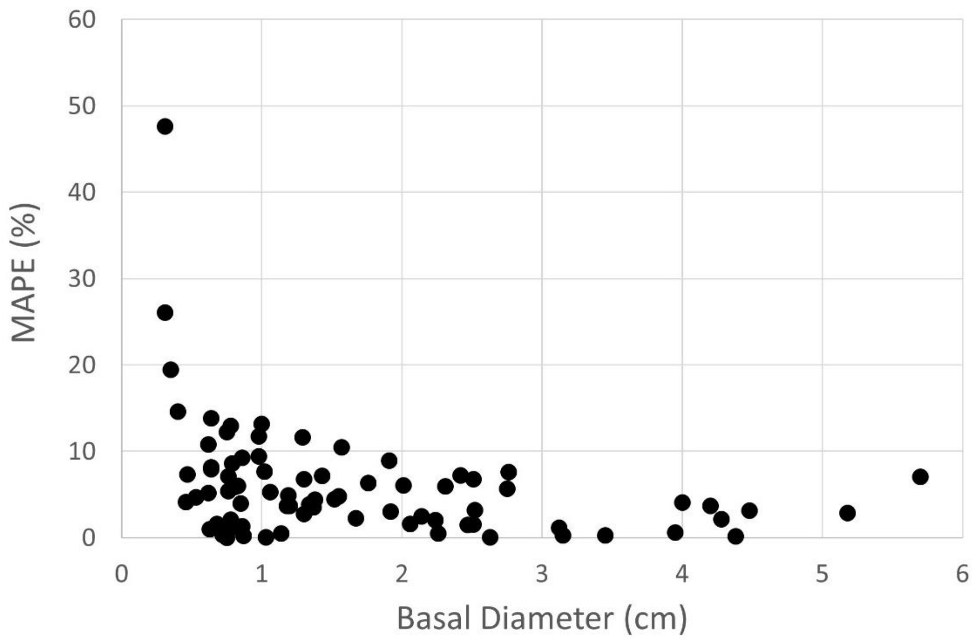

Figure 2.5: *The mean average percentage error (MAPE) for each sample based on the generalized equation.*

iii. In Section 2.3.3.1, the following sentence was changed from

"*We elected to use non-linear models, which assume normally distributed and additive errors, over log-transformed linear models, which assume log-normally distributed and multiplicative errors, for two reasons.*"

to

"We elected to use non-linear models, which assume normally distributed and multiplicative errors, over log-transformed linear models, which assume log-normally distributed and additive errors, for two reasons."

iv. The examining committee suggested the addition of the raw data tables for each genus into the manuscript (Figure 2.6).

Figure 2.6: *Raw data for the development of the allometric equations.*

Sample ID	Genus	Site	Stem Length (cm)	Basal Diameter (cm)	Dried AGB (g)
A1-A	Alnus	1	90.5	0.721	26
A1-C	Alnus	1	187	1.289	59
A1-D	Alnus	1	266	3.45	883
A2-A	Alnus	1	131	1.565	92
A2-B	Alnus	1	136	1.016	42
A2-C	Alnus	1	89	0.643	16
A2-D	Alnus	1	212	2.63	469
A3-A	Alnus	1	139	2.14	258
A3-B	Alnus	1	134.5	1.3	72
A3-C	Alnus	1	91.5	0.68	21
A4	Alnus	1	122	1.52	111
A5-A	Alnus	1	258	2.468	374
A5-B	Alnus	1	192	1.35	90
A5-C	Alnus	1	292	2.258	325
A6-A	Alnus	1	267	2.058	298
A6-B	Alnus	1	229	1.38	137
A7-A	Alnus	1	131	0.98	34
A7-B	Alnus	1	213	1.55	114
A7-C	Alnus	1	291	3.15	719
A7-D	Alnus	1	281	5.7	1595
A8	Alnus	1	389	4.38	1466
A9	Alnus	2	545	4.48	1983
A10	Alnus	2	453	3.95	1228
A11	Alnus	2	381	3.12	643
A12	Alnus	2	548	5.18	2718
A13	Alnus	2	470	4.28	1651
A14	Alnus	2	530	4.2	1782
DB1-A	Betula	1	121.5	1	34
DB1-B	Betula	1	97.1	0.791	24
DB1-C	Betula	1	53.5	0.345	7

DB2	Betula	1	135	0.872	39
DB3	Betula	1	115	0.975	36
DB4-A	Betula	1	118.5	0.69	24
DB4-B	Betula	1	169	1.37	129
DB5-A	Betula	1	203	1.34	124
DB5-B	Betula	1	179	1.14	73
DB6-A	Betula	1	67	0.46	9
DB6-B	Betula	1	89	0.75	19
DB6-C	Betula	1	107	0.78	28
DB7-A	Betula	1	115.5	0.64	16
DB8	Betula	1	250	1.3	110
DB9-A	Betula	1	105	0.764	24
DB9-B	Betula	1	119	0.785	33
DB9-C	Betula	1	39	0.309	6
DB10-A	Betula	1	67	0.62	14
DB10-B	Betula	1	130	0.825	44
DB10-C	Betula	1	133	0.85	43
DB11	Betula	1	121	0.81	27
DB12-A	Betula	1	97	0.62	21
DB12-B	Betula	1	67	0.4	9
DB13-A	Betula	1	137	0.76	37
DB13-B	Betula	1	96	0.78	21
W1-A	Salix	1	86	1.064	30
W1-B	Salix	1	87	0.314	14
W1-C	Salix	1	88.5	0.789	26
W2	Salix	1	124	0.765	26
W3	Salix	1	122.5	0.86	36
W4-A	Salix	1	178	1.2	95
W4-B	Salix	1	189	0.96	52
W4-C	Salix	1	209	1.18	92
W4-D	Salix	1	132	0.66	22
W4-E	Salix	1	132	0.75	28
W5-A	Salix	1	73	0.72	20
W5-B	Salix	1	105	0.85	28
W5-C	Salix	1	128	1.06	50
W6-A	Salix	1	126	1.19	99
W6-B	Salix	1	98	0.9	46
W6-C	Salix	1	88	0.73	16

W7-A	Salix	1	80	0.71	21
W7-B	Salix	1	104	0.5	11
W7-C	Salix	1	64.5	0.64	14
W7-D	Salix	1	125.5	0.84	79
W8	Salix	1	120	0.86	28
W9-A	Salix	1	92	0.47	8
W9-B	Salix	1	107	0.76	23
W9-C	Salix	1	133	0.63	18
W9-D	Salix	1	146	1.67	190
W10-A	Salix	1	92	0.5	13
W10-B	Salix	1	117	1.075	68
W10-C	Salix	1	202	1.736	179
W11-A	Salix	1	162	2.012	187
W11-B	Salix	1	193	1.795	237
W11-C	Salix	1	201	2.24	369
W12	Salix	1	146	2.31	337
W13	Salix	1	146	2.31	253
W14	Salix	1	130	1.03	57
W15-A	Salix	1	63	0.53	11
W15-B	Salix	1	60	0.4	7
W16	Salix	2	185	2.51	386
W17	Salix	2	423	2.42	621
W18	Salix	2	277	1.69	222
W19	Salix	2	242	1.43	173
W20	Salix	2	280	1.92	275
W21	Salix	2	440	4	1635
W22	Salix	2	370	2.52	523
W23	Salix	2	450	2.75	757
W24	Salix	2	416	2.24	600
W25	Salix	2	346	2.51	658
W26	Salix	2	336	1.91	390
W27	Salix	2	320	1.76	272
W28	Salix	2	243	1.16	78

Chapter Three: Mapping aboveground biomass of peatland shrubs using Unmanned Aerial Vehicles

3.1 Abstract

Aboveground biomass (AGB) estimation using remote sensing technologies has been widely explored in the literature, but very few studies have quantified peatland shrubby biomass and none have done so using unmanned aerial vehicles (UAVs). In this study, optical data from a UAV was used to obtain spectral (e.g. vegetation indices) and structural information (e.g. canopy height) of a shrubby fen site in Alberta, Canada. Thirty shrubs were destructively harvested and used as the calibration data for the development of an AGB model. Simple linear regression analysis was used to determine which spectral or structural variable was the best predictor of AGB. Our results indicated that structural variables, specifically UAV-derived volume (R^2=0.89) were better predictors of AGB compared to spectral variables (R^2=0.0-0.27). UAV-volume was used as the independent variable for our aboveground biomass model and this model was used to map all the shrubs across the site. We estimated a total AGB of 53 854.2kg with a mean average error of 421.05 g across a 2-ha site.

3.2 Introduction

Peatlands – wetlands that accumulate organic matter – store approximately one-third of Earth's soil carbon, while occupying just 3% of the land surface (Tarnocai, 2006; Tarnocai et al. 2009). While the wet, anoxic conditions that promote peat accumulation occur in many places (Lappaliainen, 1996), the vast majority of peatlands are found in the northern hemisphere's boreal/taiga biome (Wieder et al., 2006). Unfortunately, peatlands are very sensitive to disturbances, including changes to climatic conditions (Vitt et al., 2009) where an increase in air temperature can lead to water-table drawdowns that can alter a region's ability to store carbon

(Robinson and Moore, 2000; Tarnocai, 2006; Limpens et al. 2008; Adkinson et al., 2011; Blodau and Siems, 2012). Northern latitudes are particularly vulnerable to global warming (IPCC, 2007), making it essential to monitor Canadian peatlands, which may become a significant source of greenhouse gas emissions (Munir et al., 2014).

Estimating above-ground biomass (AGB) in vegetation is necessary for measuring total biomass and biomass production in peatlands (Korrensalo et al., 2018). In addition, AGB can provide indirect information on water levels, greenhouse gas exchange, and other site factors such as nutrient availability and land-use change (Couwenverge et al. 2011). To date, the majority of AGB studies in peatlands have relied on destructive sampling (e.g., Camill et al., 2001) or allometric equations (e.g. Conolly & Grigal, 1983; Brand & Smith, 1985; Repola, 2009). While these approaches are generally considered the most accurate means of estimating AGB (Seidel et al. 2011), they are extremely time-consuming and difficult to scale. Alternatively, remote sensing provides a more efficient strategy over large areas (Lu et al., 2016).

Gleason & Im (2011), Zolkos et al. (2013), and Lu et al. (2016) provide reviews summarizing the use of remote sensing for estimating biomass across all ecoregions. Table 1.1 lists examples of biomass estimation studies using different sensors, and forms the basis for the brief literature review that follows.

Table 3.1: *Selected examples of biomass estimation studies using spectral or structural variables. The performance of each study was based on the author's assessment of the accuracy. There was no quantitative measure that separates each category. Any study that has "conflicting" marks studies where there were mixed results on the performance of each sensor to estimate above ground biomass.*

Source	**Ecoregion**	**Sensor**	**Type of Variable**	**Performance**
Bendig et al (2015)	Agricultural field – Barley	Optical/Spectrometer	Spectral	Conflicting
Clark et al (2011)	Tropical rain forest	Optical/HYDICE	Spectral	Bad
Dong et al (2003)	Boreal and temperate forest	Optical/AVHRR	Spectral	Good
Du et al (2010)	Bamboo forest	Optical/Landsat	Spectral	Good
Foody et al (2003)	Tropical Forest	Optical/Landsat	Spectral	Conflicting
Gasparri et al (2010)	Subtropical forest	Optical/Landsat	Spectral	Conflicting
Gerylo et al (2002)	Upper Mackenzie	Optical/Landsat TM	Spectral	Good
Hall et al (2006)	Upper & Lower Foothills, Subalpine, Montane	Optical/Landsat ETM+	Structural	Good
Hame et al (1997)	Boreal coniferous forest	Optical/AVHRR	Spectral	Good
Jakubauskas & Price (1997)	Temperate coniferous forest	Optical/Landsat	Spectral	Good
Labrecque et al (2006)	Newfoundland – Long Range Mountains	Optical/Landsat ETM+	Spectral	Good
Lu et al (2004); Lu & Batistella (2005)	Brazilian Amazon	Optical/Landsat	Spectral	Conflicting
Lucas et al (2000)	Coniferous forest	Optical/Spectrometer	Spectral	Good
Li et al (2010)	Amazon Basin	Optical-Landsat	Structural	Conflicting
Main-Knorn et al 2013	Coniferous forest	Optical/Landsat	Spectral	Good
Powell et al 2010	Arizona and Minnesota	Optical/Landsat	Spectral	Good
Soenen et al (2010)	Mountainous terrain	Optical/SPOT	Spectral	Conflicting
Steininger (2000)	Tropical secondary forest	Optical/Landsat	Spectral	Conflicting
Swain et al	Agricultural field-Rice crop	Optical/Spectrometer	Spectral	Good
Tilly et al (2015)	Agricultural Field-Barley	Optical/Spectrometer	Spectral	Conflicting
Turner et al (1999)	Temperate zone	Optical/Landsat	Spectral	Conflicting
Zheng et al (2004)	Northern Wisconsin	Optical/Landsat	Spectral	Good
Abdollahnejad et al (2018)	Monoculture of 140-year-old *Pinus sylvestris* L.	UAV-RGB	Structural	Good
Asner et al (2009); Asner (2012); Asner & Mascaro, (2014)	Tropical Rainforest	Lidar	Structural	Good
Bendig et al (2014)	Agricultural field – Barley	UAV-RGB Camera	Structural	Good
Chen et al (2012)	Experimental forest	Lidar	Structural	Good
Naesset & Gobakken (2008)	Boreal Forest	Lidar	Structural	Good
Greaves et al (2015)	Arctic tundra	Lidar	Structural	Good
Lefsky et al (1999)	Western Hemlock Forests	Lidar	Structural	Good
Lim et al (2003)	Northern hardwood forest	Lidar	Structural	Good
Lu et al (2012)	Sierra Nevada	Lidar	Structural	Good

The most common procedures involve optical reflectance measurements (also referred to as spectral variables) such as vegetation indices (VIs) from satellite or piloted-aircraft platforms (Lu et al., 2016). VIs have been commonly used because they remove the variability caused by external factors such as canopy geometry and soil background (Blackburn & Steele, 1999; Gao et al., 2000; Boegh et al., 2002). Two main challenges with using spectral variables as AGB estimators are: 1) the performance of spectral variables vary across different sites and 2) spectral sensors have a low data saturation point. For example, Jakubaukas and Price (1997) found strong relationships between AGB and the Landsat Thematic Mapper (TM) band 7 (shortwave infrared) and the normalized difference vegetation index (NDVI) in the lodgepole pine-dominated forests of Yellowstone Provincial Park. In contrast, Hame et al. (1997) found NDVI to be a weak predictor and that the red band was the most suitable for ABG estimation in Finland's boreal forest. Other studies have found that the data saturation problem in optical sensors has caused issues in using spectral variables as predictors of AGB. For example, Lu et al (2005) evaluated the performance of spectral variables across three study areas in the eastern Amazon basin. They found that spectral variables were strongly correlated with forest stand parameters until biomass reached approximately 15 kg/m^2 or successional age exceeded 15 years. Spectral bands would saturate, past this point, which weakened the correlation with forest stand parameters. Bendig et al. (2015) made a similar observation in barely crops where the accuracy of biomass estimates significantly decreased after crops have reached a certain height.

Light Detection and Ranging (lidar) sensors have been identified as the most accurate method for mapping AGB because of the structural information one is able to obtain through these sensors. Lidar-generated point clouds provide a 3D representation of the area of interest. From these point clouds, one is able to obtain vertical and horizontal information. Several researchers have found that structural information derived from 3D point clouds provide strong predictors of AGB, even outperforming their VI alternatives in some instances (Tilly et al., 2015; Clark et al., 2011). For example, Tilly et al. (2015) studied the performance of lidar-derived plant height compared to six vegetation indices. Plant height performed as a strong estimator (R^2 up to 0.89) whereas individual VIs showed varying performances (R^2=0.07-0.87). Clark et al. (2011) also tested structural parameters derived from lidar versus hyperspectral metrics and found that the lidar metrics provided a higher accuracy in estimating biomass. Structural variables have been found to be good predictors of AGB across a variety of ecoregions. For example, vegetation height has performed well in temperate coniferous forests (Popescu et al., 2004; Ota et al., 2017), agricultural fields (Yin et al., 2011; Bendig et al., 2014; Tilly et al., 2015; Madec et al., 2017;), tropical forests (Ota et al., 2015), and arctic tundra (Greaves et al., 2016; Fraser et al., 2016).

Recent progress in Unmanned Aerial Vehicles (UAV) based imaging has opened up new windows for research and investigation. UAVs are particularly attractive because of their capacity to generate high-density point clouds (DPC) based on photogrammetric principles and structure from motion (SfM) workflows (Sturm & Triggs, 1996). Optical cameras are typically mounted on UAVs to retrieve both structural, through the DPCs, and spectral information. This is a noteworthy advantage of the UAV platform because it addresses the challenges encountered by other platforms and sensors. For example, lidar and Radio Detection and Ranging (radar) sensors are unable to collect spectral information whereas optical sensors are unable to collect vertical structural information. Previous research has demonstrated that UAVs are able to measure structural-vegetation parameters, such as vegetation height, at accuracies comparable to lidar (e.g., Dandois & Ellis, 2013; Fraser et al., 2016; Ota et al., 2017; Madec 2017; Goodbody et al., 2017; Hird et al., 2017; Van Iersel et al., 2018). Other studies have also demonstrated how UAV can be used in AGB estimation in crops (Bendig et al., 2014; Yue et al., 2017) and woodlands (Puliti et al., 2015; Kachamba et al., 2016).

While biomass estimation has been widely explored in the remote-sensing literature, relatively fewer studies have focused on peatlands. One challenge associated with peatland AGB studies is that a large proportion of peatland vegetation communities (up to 88% in continental boreal sites) are comprised of multi-stemmed shrubs (Campbell et al., 2000). Compared to trees, shrubs have received little attention from the remote-sensing community due to their low economic value (Estornell et al 2011; Greaves et al 2015). Besides, their unique physical attributes (e.g., low height, uniform surface) makes it difficult to assess using traditional remote sensing approaches of ABG estimation (Estornell et al 2011; Greaves et al 2015). As a result, there is a need for new remote-sensing techniques specifically aimed at estimating shrubby AGB in peatlands using high spatial resolution imagery (Estornell et al, 2011; Olsoy et al 2014; Greaves et al., 2016). A search of the literature revealed just two studies that used radar backscatter values to estimate AGB in peatlands (Englhart et al., 2011; Peregon & Yamagata 2013). Peregon & Yamagata (2013) used HV-polarized backscatter that resulted in a coefficient of determination (R^2) between 0.35-0.49 and root mean squared error (RMSE) between 25%-32% of mean biomass. Englhart et al. (2011) used a combined model of L- and X-band SAR and achieved an R^2 of 0.53 with an RMSE of 79 t/ha across 400 independent validation points. The use of radar sensors is promising because of its ability to penetrate beneath the forest canopy, though data saturation can be an issue (Lucas et al., 2007; Solberg et al., 2010). Additionally, rough land surfaces can cause for speckle in radar data and would require extensive noise filtering to be able to improve vegetation height estimation (Kellndorfer et al. 2004).

To date, no studies have assessed the value of unmanned aerial vehicles (UAVs) as a platform for estimating AGB in peatlands. However, UAVs have been shown to provide accurate depictions of other important attributes such as microforms (Mercer and Westbrook, 2016; Lovitt et al., 2017) and groundwater levels (Rahman et al., 2017), and are likely capable of producing peatland-AGB maps at unprecedented levels of detail.

The purpose of this study was to develop strategies for estimating shrubby AGB in a peatland site located in northwestern Alberta, Canada, using UAV data. In particular, we set out to compare the relative value of spectral (VIs) and structural (point cloud) variables for measuring shrubby AGB, using a sample of individuals selected for destructive harvesting. Once the most effective predictor was determined, we then produced a high-quality map of above-ground shrub biomass across our 2-hectare study area. The work represents the first-known use of UAVs to estimate shrubby biomass in peatlands.

3.3 Methods

3.3.1 Study Area

The study site is a shrubby fen located ~100 km southeast of Peace River, Alberta (56°06'04.0"N 116°41'23.0"W) covering ~2 ha of land area (Figure 3.1). It falls within the Dry Mixedwood natural subregion with a mean annual temperature of 1°C and mean annual precipitation of 46.1 cm (Natural Regions Committee, 2006). The dominant shrubs on this site are alder (*Alnus* spp.), willow (*Salix* spp.), and bog birch (*Betula pumila*). The height of these shrubs ranges from 30 cm to 4 m. Sedges and various species of mosses such as *Aulocomnium palustris*, *Tomentypnum nitens*, *Helodium blandowii*, and *Plagiomnium ellipticum* dominate the understory vegetation.

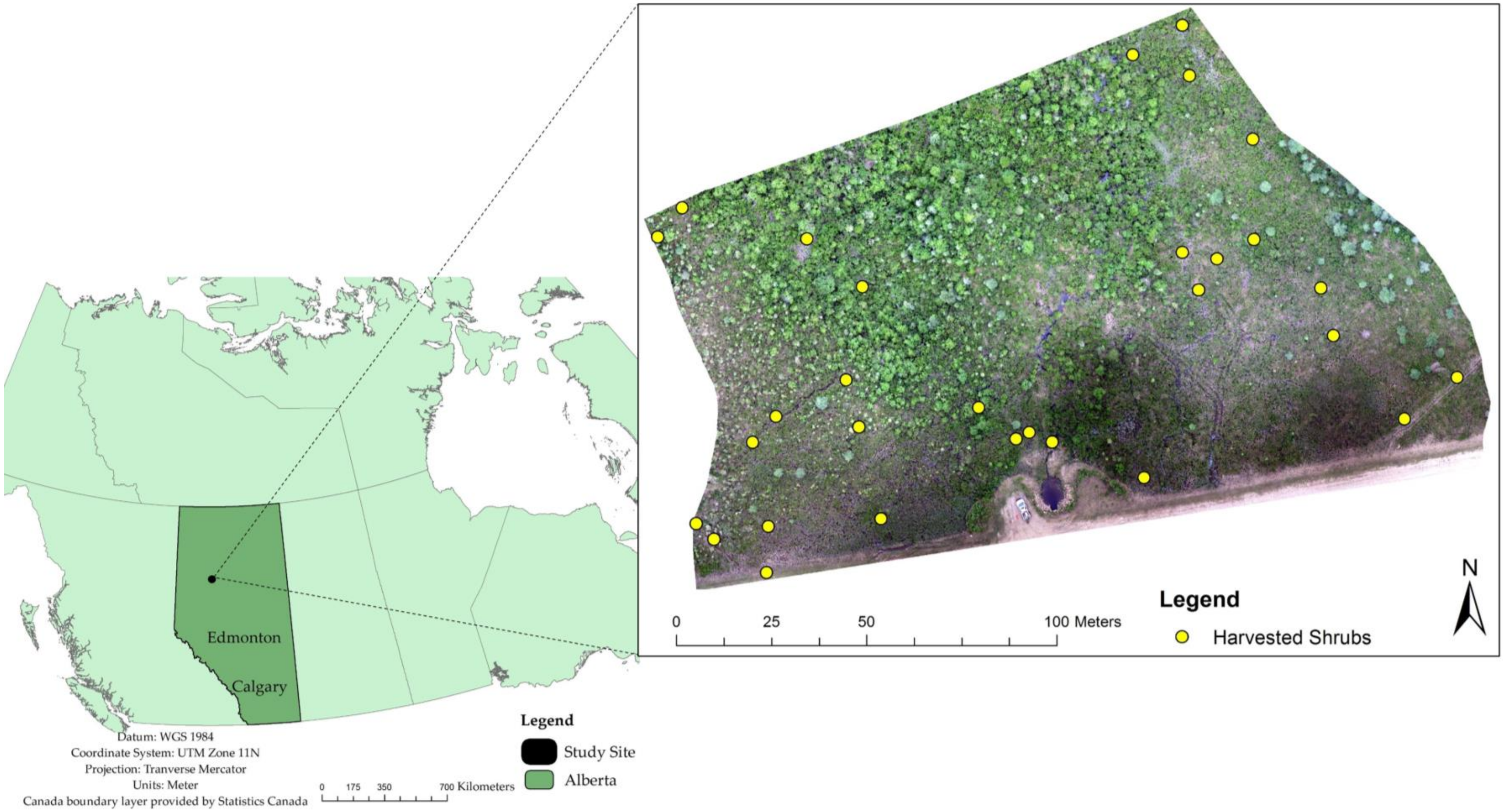

Figure 3.1: *An orthophotograph of the study area with its geographical position on a map of Canada. The locations of each harvested shrub are displayed on the orthophoto as yellow points (right).*

3.3.2 Data Collection

3.3.2.1 Description of data sets

Two types of data were collected for this study: (i) field data, and (ii) remote sensing data. The field data collection included field measurements (height, width, etc.) and destructive sampling of shrubs to measure actual biomass. These field data were then used to develop remote sensing-based biomass estimation model and to evaluate the accuracy of the model. The remote sensing data included UAV-based orthophotos and photogrammetric point clouds that were collected from three flight missions. The following section describes the datasets in detail.

3.3.2.2 Field Data

Field data collection was performed between June 5, 2018, and June 7, 2018. It included two main steps: (i) preliminary reconnaissance survey, (ii) detail measurement of shrub structure and destructive sampling. The preliminary reconnaissance survey was performed on June 5 2017, which involved walking across four east-west transects traversing the study area spaced 25 m apart. The location of all well-isolated shrubs within one meter of the transects were recorded using a Garmin Montana 600 handheld GPS. We targeted well-isolated shrubs to ensure that they could be confidently identified in the associated remote-sensing data. The preliminary survey resulted in a list of 50 individual shrubs with a record of each shrub's location, height, and genus. From this list, the shrubs that would be harvested were chosen based on a stratified random sampling approach to ensure spatial and genus variability. To do this, the study site was divided into four quadrants and 8 samples per quadrant were chosen. Within each quadrant, samples were stratified again by genus where we randomly chose 2 samples per genus; however, some quadrants did not have any alders or bog birch which resulted in more willows being chosen (Table 3.2).

Table 3.2: *Descriptive statistics of the harvested shrubs*

Genus	n	Height range (m)	Average Height (m)	Average Number of stems per shrub	Biomass range (g)	Average AGB (g)
Alder	7	2.2 - 3.7	3.1	7	32-3098	1193
Willow	15	1.0 - 2.2	1.6	27	115-3433	888
Bog Birch	8	0.8- 2.6	1.5	26	172-2139	744

On June 7, 2017, the location of the chosen shrubs was recorded again using a survey-grade Trimble R4 RTK GNSS system prior to harvesting the shrubs on the same day (Figure 2.1). The Trimble R4 RTK GNSS system has centimeter-level accuracy which is more precise compared to the previously used handheld GPS. Shrub height and shrub width, number of stems, basal diameter of stems, and stem length were recorded in the field or in the laboratory for each harvested shrub. The height and width of each shrub was measured using a standard measuring tape that could measure to the closest centimeter. Samples were stored for no longer than two days at 4°C then dried at 70°C until a constant mass was reached. The leaves and stem were separated and weighed with a Denver Instrument SI-6002 scale (that measured to the nearest gram) to obtain the biomass of the samples.

3.3.2.3 Remote Sensing Data

All flights were conducted with the Sensefly's Ebee Classic and associated eMotion 3 software; the specifications for this UAV and flying parameters can be found in Table 3.3. One leaf-off flight was flown on April 21, 2017 and two leaf-on flights were flown on June 7, 2017. All missions were flown in overcast conditions, at a height of 75 m to obtain 2.5 cm ground-sample distance. The overcast conditions minimized the influence of shadows, which can cause unusable "no data" gaps in airborne data sets. Perpendicular flight lines were configured across the site to generate 80% forward overlap and 60% lateral overlap. The images from the leaf-off flight was collected using a Canon S110 RGB camera; they were used to build a digital terrain model (DTM) of the study area. The Canon S110 RGB camera and the Canon S110 RE camera were each flown in leaf-on conditions prior to harvesting the shrubs. The RGB images from the before harvest flight was used to build the digital surface model (DSM). Six ground control points (GCPs) were distributed systematically across the study area. All GCPs were surveyed with the same RTK GNSS system that was used to survey shrub locations.

Table 3.3: *Specifications of the unmanned aerial vehicle (UAV)*

Model	**Ebee Classic**
Manufacturer	Sensefly
Wingspan	96 cm
Weight	~0.69kg
Camera	Canon S110 RGB Canon S110 Red Edge
Camera specifications	Type: 12.1 Megapixel, 1/1.7-inch CMOS Focal Length: 5.2 (W) – 26.0 (T) mm Maximum Aperture: f/2.0 (W)-f/5.9 (T) Shutter Speed: 1-1/2000 sec, 15-1/2000 sec (in Tv and M modes) Sensitivity: Auto, ISO 80-128000 Dimensions: 98.8x 59.0 x 26.9 mm
Cruise speed	40-90 km/h
Wind resistance	Up to 45 km/h
Max. flight time	50km
Max flight range	33 km
Flight planning & control software	eMotion 3

3.3.3 Model Development

Figure 3.2 shows a general workflow of how the data from each flight mission was used to develop the AGB model and an AGB map for the study area.

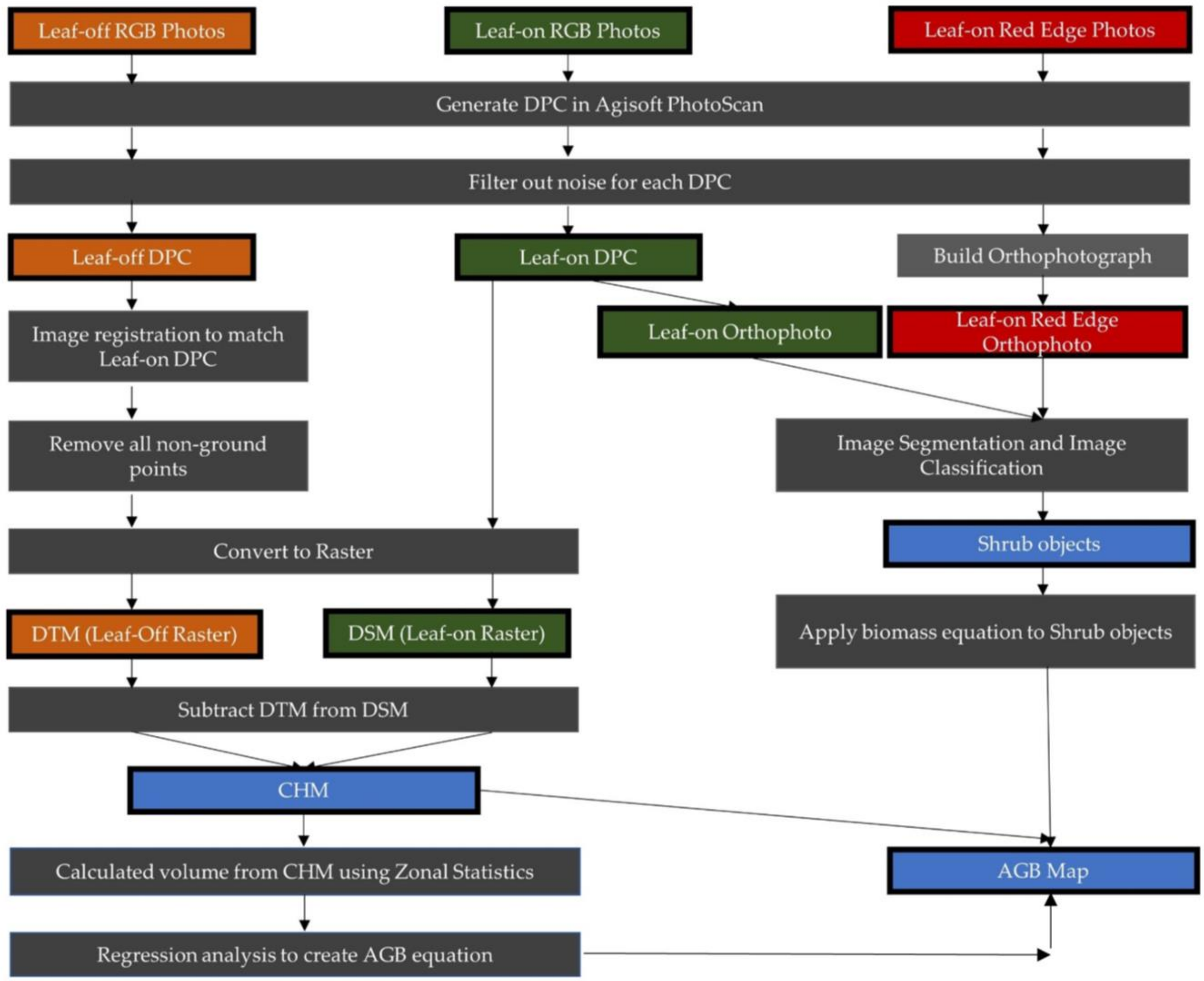

Figure 3.2: *Workflow for mapping above ground biomass (AGB) using imagery collected from unmanned aerial vehicles. The colored boxes represent inputs or outputs and the grey boxes represent processing steps.*

3.3.3.1 Image Processing

Agisoft PhotoScan Version 1.2.4 was used to generate a dense point cloud (DPC) and a digital orthomosaic from the UAV photographs. Agisoft Photoscan uses the SfM workflow where a DPC is generated through the detection of common reference points amongst overlapping photos taken from different locations. The leaf-off optical flight had 101 photos, leaf-on optical flight had 74 photos, and the leaf-on red edge flight had 90 photos. Photo quality was assessed using Agisoft Photoscan photo-quality assessment tool and low quality photos were removed (< 0.5). Photos were aligned using camera positions and geo-referenced with the 6 GCPs for each flight. The average XY (vertical and horizontal) error for the leaf-off DPC was 0.007 m and 0.143 m for the leaf-on DPC (Table 3.4). All DPCs were generated under the high-quality setting and a mesh was built to generate an orthophotograph. Outliers were removed from the DPCs and then the DPCs (from optical images) were exported into CloudCompare software.

The leaf-on DPC and the leaf-off DPC were geo-referenced with different GCPs, which resulted in a slight horizontal offset. In order to fix this offset, the image-registration tool in CloudCompare 2.7.0 software package was used to alter the leaf-off DPC to align with the leaf-on DPC through the manual identification of GCPs. The RMSE for the image registration was 0.341m (Table 3.4). A visual assessment was done to ensure that there was an improvement in the matching of the DPC. Table 3.4 summarizes the RMSE for all point clouds including the image registration.

Table 3.4: *Summary of the accuracies of the geometric rectifications for the dense point clouds and image registration. The type of validation column indicates how each dataset was rectified and reports the root mean squared errors (RMSE) of vertical and horizontal accuracies.*

Dataset	Type of validation	RMSE (m)
Leaf-off DPC	Ground control points	0.007
Leaf-on DPC	Ground control points	0.143
Image Registration of Leaf-on DPC and Leaf-off DPC	Manual identification of matching points	0.341

The LASground tool, found in LAStools version 160110, was used to classify the leaf-off DPC points into ground points (class =2) and non-ground points (class=1) based on a set of user-defined parameters. The software also has default settings for different landcover types (e.g. wilderness, city, nature, etc.); we used the parameters for the “wilderness” setting for our initial ground classification. After majority of surface points had been removed, we overlaid the orthophotograph with the remaining ground points, and manually reclassified points that were non-ground.

The leaf-on DPC (all points) and the leaf-off DPC (only ground points) were converted to raster with a 2.5 cm pixel size; the output was the DSM and DTM, respectively. Then, the DTM was subtracted from the DSM to create the canopy height model (CHM).

3.3.3.2 Accuracy assessment of canopy height model

Prior to regression analysis for the UAV-structural variables, the accuracy of the UAV-CHM was first assessed. Figure 3.3 shows a comparison between the heights of the shrubs measured in the field and the heights derived from the UAV. Shrub height in the UAV-data was represented by the maximum height within each shrub polygon found in the CHM. The R^2 for this comparison was 0.68 with a standard error (SE) of 0.43. The standard error (SE) was calculated as

$$SE = \frac{RSS}{N-1} \tag{2}$$

Where, *RSS* is residual sum of squares and *N* is the number of samples. The regression line has a y-intercept of 0.97, which indicates that the CHM (from UAV) is generally underestimating the field heights. In Figure 3.3, majority of data points fall above the reference line which indicates a pattern of underestimation across all samples. We suspect that this pattern across UAV shrub heights is caused by the misidentification of ground points used to generate the DTM. Our study area is densely vegetated with grasses which may have prevented "true" ground points from being identified and used for the DTM. This error appears to systematic and we do not believe it will affect the accuracy of our AGB model.

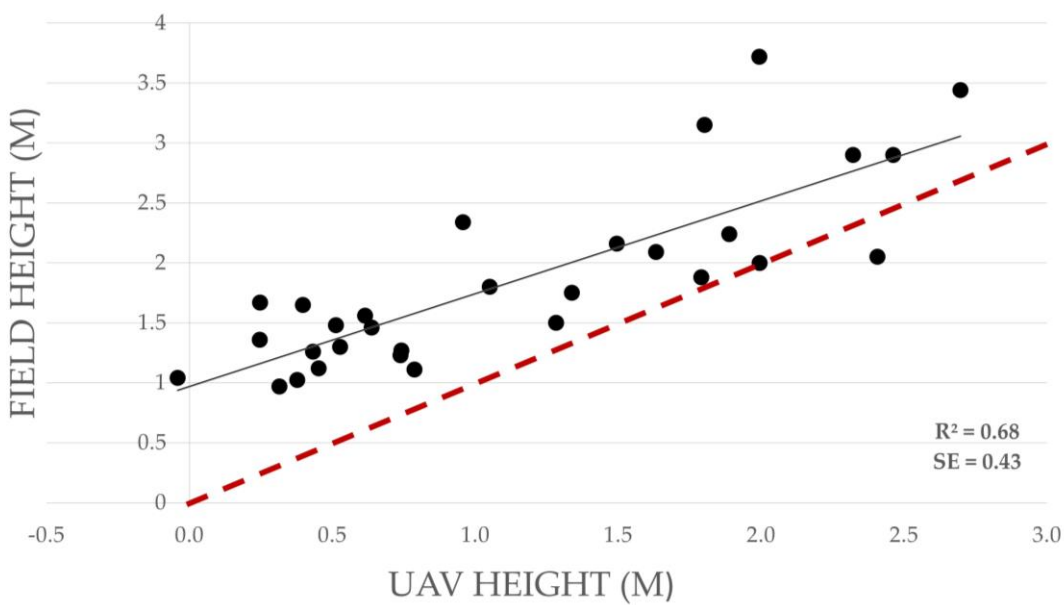

Figure 3.3: *A comparison of the field-measured height (m) with the UAV-derived height (m) for the thirty harvested samples. The coefficient of determination (R^2) and standard error of the estimates (SE) are reported. A 1:1 reference line is marked by the red dotted line.*

3.3.3.3 Predictor Variables

Three sets of predictor variables were identified for estimating AGB: (i) field data based structural variables, (ii) UAV based structural variables, and (iii) UAV based spectral variables.

The GPS coordinates of the harvested shrubs were used to find each individual shrub on the ortho-image. We then created a polygon for each shrub by manually outlining it on the ortho-image. UAV-structural parameter values (average height, maximum height, and sum of heights) of these shrubs (polygons) were obtained using Zonal Statistics tool on CHM (raster) in ArcGIS. We considered the sum of all pixel values to be representative of the volume of the shrub, because it captures the height for each pixel that falls within in shrub polygon (see Figure 3.4).

The four spectral variables chosen were the red edge band, red band, simple ratio (SR), and normalized distance vegetation index (NDVI); the SR and NDVI indices have both been identified as being strongly associated with AGB (Chen, 1996; Mutanga & Skidmore, 2004; Mutanga et al 2011). We did not have access to a NIR camera, therefore, the red edge camera was used to calculate vegetation indices. The red edge band is defined as the zone in the spectrum where there is a rise in reflectance at the boundary between the chlorophyll absorption in the red wavelength and leaf scatter in the NIR wavelengths (600-750 nm). The UAV- spectral variables for each shrub was also derived using Zonal statistics, with the optical bands and red edge bands as the raster input.

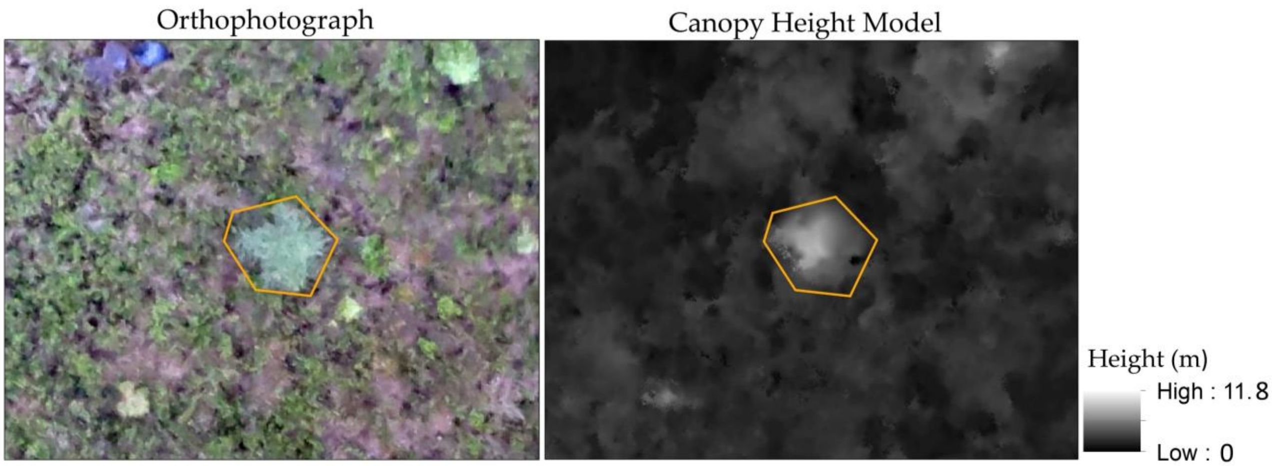

Figure 3.4: *Representation of how volume is derived from UAV-imagery. Each pixel has an associated height value assigned to it. To calculate the volume, the sum of all height values that fall within the shrub boundary was calculated.*

3.3.3.4 Statistical Analysis

Linear regression analysis was used for all field and UAV-derived variables with AGB as the dependent variable in IBM SPSS Statistics 27 software. All equations for estimating aboveground biomass (M) were in the form as

$$M = bX + a \tag{1}$$

where *a* and *b* are the fitted coefficients and X is the structural or spectral variable. Linear regression models are commonly used across AGB models with remote sensing variables (Lu et al., 2016). The predictor variable with the highest R^2 value was chosen to be used in the AGB equation.

3.3.4 Model Application and Map Development

The AGB equation was applied to all shrubs in the study site. An RGB orthophotograph of the study site was used as the input for object-based classification of land cover types. The AGB was only applied to shrub objects. eCognition Developer 64 software package was used to segment and classify the image into three landcover types: water, grass, and shrubs. The leaf-on orthophotograph, the CHM, and the red-edge orthophotograph were overlaid into one image file to include all layers in the image segmentation process. Multiresolution segmentation was used to define objects and then decision rules were used to assign a class to each image segment (see Figure 3.5).

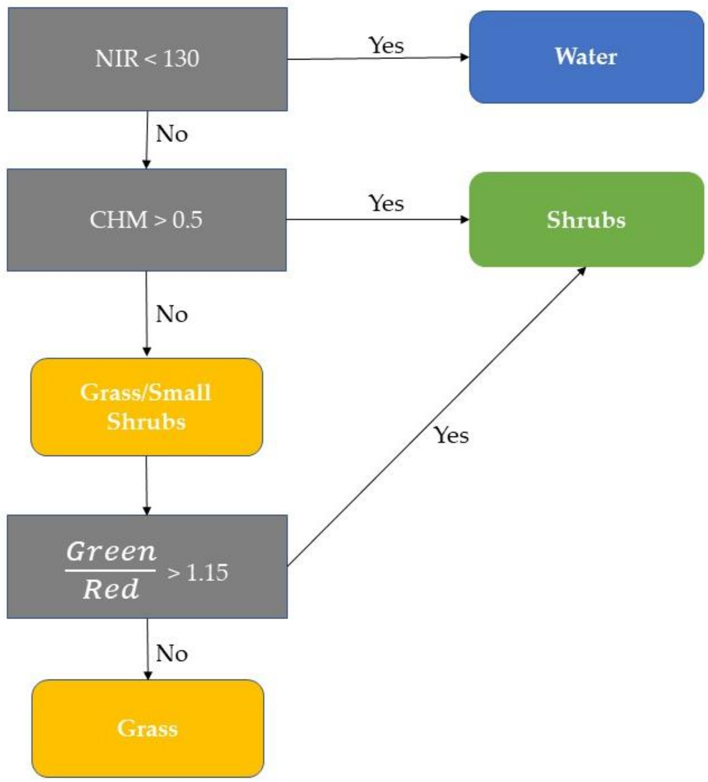

Figure 3.5: *A visual representation of the decision tree and associated thresholds used in eCognition Developer 64 for the classification of objects into three classes (water, shrubs, and grass).*

A confusion matrix was generated to validate the classification (Figure 3.6) using 50 randomly chosen reference pixels for each land cover class, which were extracted using visual image interpretation. We obtained an overall accuracy of 80%, which was deemed sufficient to move forward. The shrubs class was not further refined by species or genera because a previous study, on the same site, which showed that genus information was not required to obtain accurate biomass estimates (He et al., 2018; Chapter 2). He et al (2018) demonstrated that a generalized model was able to accurately estimate AGB based on basal diameter (R^2 =0.93).

The best equation from our statistical analysis was then used to calculate AGB for shrub objects across the entire study site. A 10-fold cross validation was used to partition the 30 shrub samples into training and test sets for accuracy assessment in RStudio 1.1.453.

Overall Accuracy: 79.33%
Kappa Coefficient: 0.69

Classified Pixels	Reference Pixels: Water	Grass/Ground	Shrubs	Total	User's Accuracy	Producer's Accuracy
Water	26	0	2	28	93%	52%
Grass/Ground	7	45	0	52	87%	90%
Shrubs	17	5	48	70	69%	96%
Total	50	50	50	150	-	-

Figure 3.6: *Confusion matrix of the land cover classification for the AGB map. Class sample points (ground truth data) were identified on orthophotographs by visual interpretation.*

3.4 Results

3.4.1 Comparison among different biomass prediction models

Table 3.5 reports the R^2 and RMSE of each variable for estimating AGB. In addition to the UAV-based spectral and spatial variables described earlier, we have also included models of ABG created with field-measured height and width data. Within the field data variables, height (R^2=0.705) performed better than width (R^2=0.417). Height and width were then fit into a multiple regression equation, which produced an adjusted R^2 value is 0.74 and RMSE of 744.336 g. The adjusted R^2 was used, as opposed to the R^2, because it accounts for the addition of a variable. Both variables were found to be statistically significant ($p<0.01$). Height from the field and from UAV performed similarly with R^2 values of 0.705 and 0.713, respectively.

Amongst the UAV-structural variables, volume (R^2=0.885) performed the best and mean height performed the worst (R^2=0.594). The four spectral variables all had a R^2 of less than 0.27 with the Simple Ratio VI performing the best (R^2=0.274). The results from Table 3.5 concludes that the UAV-structural variables performed better than the spectral variables. UAV-volume had the lowest RMSE and highest R^2, overall, therefore it was used as the predictor for our AGB equation.

Table 3.5*: A summary of each model's performance with dried aboveground biomass based on coefficients of determination (R^2) and root-mean-square errors (RMSE). The * indicates that an adjusted R^2 was reported because a multiple linear regression was used instead of a simple linear regression.*

	R^2	RMSE(g)
Field Data		
Height	0.705	802.359
Width	0.417	1126.763
Height & Width	0.740*	744.336
UAV – Structural Variables		
Max height	0.713	790.26
Volume	0.885	500.33
Mean height	0.594	940.56
UAV – Spectral Variables		
Red Edge	0.004	1473.67
NDVI	0.116	1388.29
Red Band	0.21	1312.01
RVI/ Simple Ratio	0.274	1257.95

3.4.2 AGB map of a shrubby fen

The linear regression equation coefficients (derived from UAV based shrub volume measurements) are reported in Table 3.6.

Table 3.6: *Model parameters for AGB linear regression with UAV-volume as the predictor variable. Standard error of the slope coefficient (b) and constant (a) are reported with the mean average error (MAE).*

b	SE[*b*]	*a*	SE[*a*]	MAE(g)
0.5776	0.04	507.34	112.11	421.05

The equation was applied to all shrub objects across the site. Table 3.7 summarizes the descriptive statistics for shrub objects. There was a total of 70793 shrub objects and the average size of each shrub (in pixels) is approximately 388. The smallest shrub object covered 111 pixels and the largest shrub covered 3574 pixels. AGB ranged from 52.5g to 6396.5g and the average biomass per shrub was 760.7g.

Table 3.7: *Descriptive statistics for shrub objects. N is the number of shrub objects in the study site. Biomass in this table refers to aboveground biomass.*

	N	**Average size (pixels)**	**Minimum Size (pixels)**	**Maximum size (pixels)**	**Minimum biomass (g)**	**Maximum biomass (g)**	**Average biomass (g)**	**Total Biomass (kg)**
Shrubs	70793	388	111	3574	52.5	6396.5	760.7	53854.2

Some “shrub” objects exhibited negative biomass values; these objects are water bodies that have been misclassified as shrubs (see Figure 3.6). Negative biomass estimates for these objects were not included in the total biomass estimate for the site. The instance of finding negative biomass values can be seen as an additional filtering tool to offset the classification error (see

Figure 3.6). For example, water objects misclassified as shrub objects would have negative biomass values, therefore, it was clear which water objects had been misclassified. The total AGB (dry weight) was calculated as approximately 3 kg/m^2 (Table 3.7 and Figure 3.7). This estimate falls within the range of shrub AGB found across the 186 peatland sites surveyed by the Canadian Forest Service in their peatland productivity and decomposition database (Bona et al., 2018). Although we were unable to harvest other shrubs that could have been used as a quantitative measurement of the map's accuracy, we believe the cross-validation of the volumetric equation and the comparison with the Canadian Forest Service AGB measurements is sufficient in demonstrating the accuracy of the AGB map.

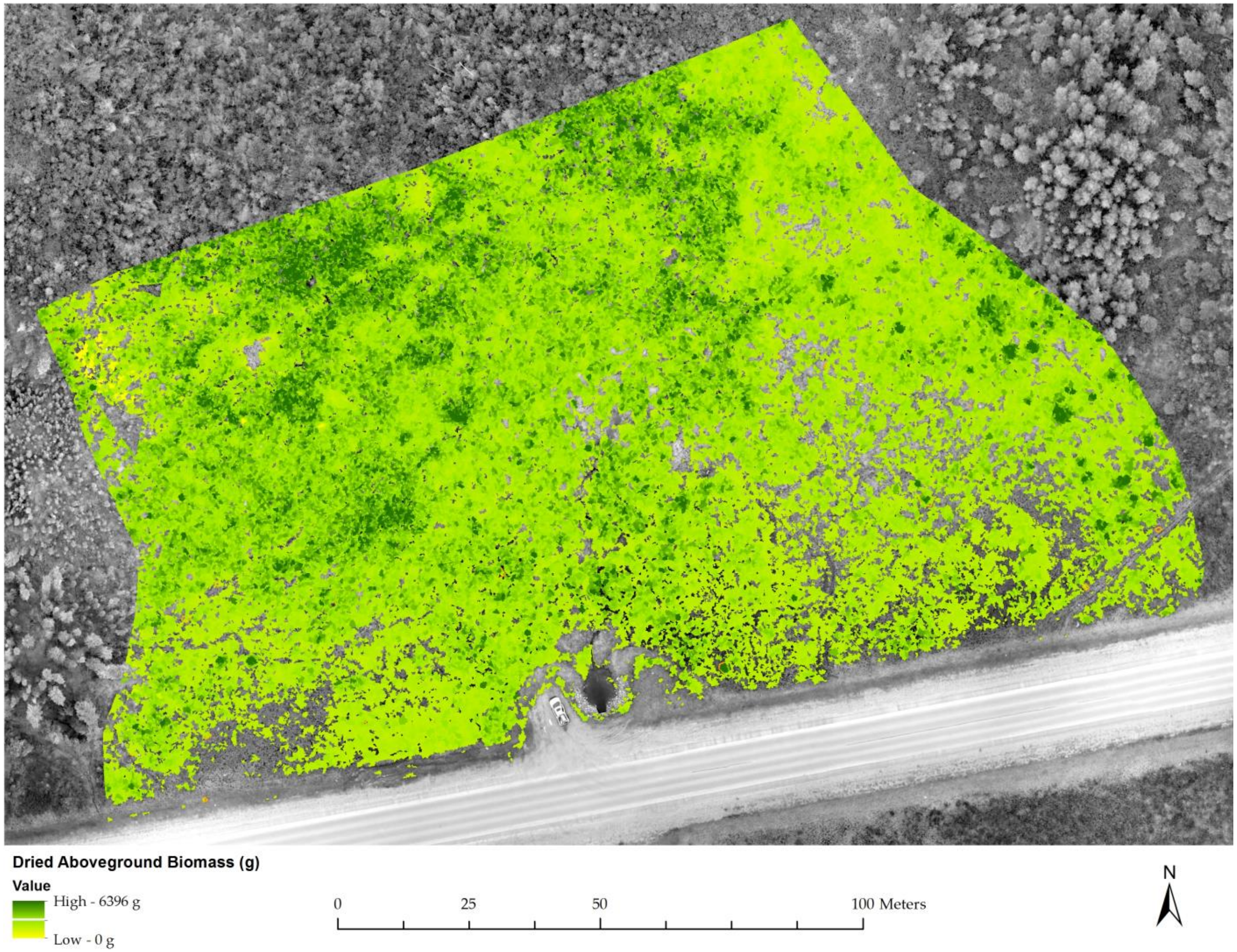

Figure 3.7 *Aboveground biomass (AGB) map generated based on a simple linear regression model with UAV-volume as the predictor. The estimated dried weight of AGB across this site is 53 854.2kg. The underlying image is an orthoimage of the study site.*

3.5 Discussion

3.5.1 Comparison of field height with UAV-derived height

The underestimation of height from the UAV-CHM is primarily due to the difficulties in generating an accurate DTM with photogrammetric point clouds. Despite attempts to obtain ground points with a leaf-off flight, the general underestimation of height shows that the ground points may not have been “true” ground points but rather low-lying vegetation or grass. Because the underestimation is consistent across all areas in the site, this is indicative of a systematic error. Figure 3.8 are field photos that demonstrate the density of the vegetation found across the study site. Shrub height was measured from the base of the tallest stem to the standing height of that same stem. Peatlands are commonly known to have uneven and undulating ground surfaces and our study site follows this characterization; stem bases (the point where the stem meets the ground), even within the same shrub, had varying elevations. Optical sensors are unable to penetrate beneath the canopy, making it difficult to capture the heterogeneity found across the ground surface.

Figure 3.8*: Field photos taken on June 15 2017. The image on the left is the field assistant measuring the width of shrub and the other image is an overview of the study site.*

Despite the underestimated UAV-height measurements, the R^2 values for field height (R^2= 0.705) and UAV height (R^2 =0.713) are similar (Table 3.5). To test whether the linear regression equation for field height with AGB and UAV height with AGB were statistically different, we tested the slope coefficient using a z test, where z values were calculated as

$$z = \frac{b_1 - b_2}{\sqrt{SEb_1^2 - SEb_2^2}} \tag{3}$$

Where, b_1 is the coefficient of model 1 and b_2 is the coefficient of model 2; SEb_1 and SEb_2 are the standard error of each model coefficient, respectively. The null hypothesis was that 'there is no difference between the coefficients being compared'. The purpose of this test was to determine if the rate of change between height and AGB is different across the two models. Table 3.8 shows that there is no significant difference between the slopes of the two models ($p > 0.05$); in other words, the relationship between field-height and AGB and UAV-height and AGB is not significantly different. This confirms that there is a systematic error across the entire study site and shows that, despite the underestimation in height, this biomass equation can be applied across the entire site.

Table 3.8: *Comparison of height to AGB models-one is height measured from field and the other is measured from UAV. Z or t scores represent differences in model slope (b).* SE_b *is the standard error of the slope coefficient. Differences are significant at the 0.05 threshold.*

b_{field}	SEb_{field}	b_{UAV}	SEb_{UAV}	Z or t score	p-value
16.44	2.01	15.53	1.86	0.33	0.74

3.5.2 AGB prediction models

We were unable to find a strong correlation with any of the spectral variables. The dense understory vegetation is a probable explanation for the poor correlation found between AGB and the spectral variables. Similar to the observations made in Mutanga & Skidmore (2004) and Bendig et al (2015), we believe the VIs had limited value in estimating biomass because of data saturation. Based on our results, we would not recommend the use of spectral variables in peatland sites.

The structural variables were all strong predictors of AGB (R^2 = 0.594 – 0.885). According to Lu et al. (2012), R^2 values for lidar-based biomass estimation studies range from 0.6 -0.9; our results are, therefore, comparable to other lidar studies. Table 3.9 lists select lidar-based biomass estimation studies and their associated R^2 values. A couple of those studies found mean height (from CHM) as a strong predictor (Lefsky et al. 2002; Asner et al, 2009). Mean height performed well (R^2=0.594) in our study site compared to the spectral variables, however, our volumetric approach was the better predictor of AGB. UAV-volume was the variable chosen to be used in the AGB equation because it had the highest R^2 and lowest RMSE. We believe that the superior performance of this variable, compared to other structural variables, is attributed to the manner in which volume is able to account for the surface area each shrub covers as well as the unique shape of each shrub. Greaves et al. (2015) and Chen et al. (2007) both made similar conclusions in their studies using lidar.

The limitation with using lidar in our peatland site is not only the cost but the point density of the available data. The ground-sample distance from the listed lidar sensors (Table 3.9) were between 0.5m – 1 m whereas the ground-sample distance from our UAV is 2.5 cm. We are confident that our shrub samples would not be visible in the data with a cell size of 0.5 m and a point density of 1 point/m^{-2} because of the dense site conditions and the relatively small size of the shrubs. Of the listed studies, Greaves et al. (2015) and Estornell et al. (2011) were the only lidar studies that estimated AGB of shrub species. They demonstrated that lidar could be used to estimate shrub biomass sufficiently (R^2=0.62 – 0.73), however, this is only under the condition where high density lidar is available.

Table 3.9: *Selected examples of studies that used structural variables as predictors for aboveground biomass (AGB)*

Study	Predictor Variable	R^2
Asner et al. (2009)	Mean Height	0.78
Chen et al. (2012)	Quadratic Mean Height	0.82
Greaves et al. (2015)	Volume	0.62
Lefsky et al. (2002)	Mean Canopy Height Squared	0.82
Lim et al. (2003)	Intensity return values	0.85
Lu et al. (2012)	Maximum height	0.77
Naesset & Gobakken (2008)	Canopy height and canopy density	0.82
Popsecu et al. (200	Height and Crown Diameter	0.33

3.5.3 Model application - scopes and limitations

3.5.3.1 Model transferability/portability

Our study, along with other biomass estimation studies (Table 3.1), have demonstrated that remote sensing has been successfully used to estimate AGB. However, the challenge of applying these models across space and time still remains. Transferability of models remains a challenge for all sensors on any platform because of the varying forest structures and environmental conditions for each study area (Lucas et al., 2015; Lu et al., 2016). This is especially difficult for optical sensors because spectral signals are affected by the biophysical environment and vegetation characteristics such as phenology, species composition, and health (Lu, 2006; Foody et al., 2003). Foody et al. (2003) attempted to transfer vegetation indices, multiple regression, and neural network models across sites and was unsuccessful in applying all three types of models outside of the region in which they were developed. We believe that structural variables may be less sensitive to external factors and show greater potential for portability in comparison to spectral variables. Lefsky et al (2002) and Asner et al (2012) are two studies that have demonstrated that biomass regression equations developed with a structural variable can be applied across multiple sites. Asner et al (2012) found that they were able to use mean canopy height after accounting for each site's wood density and basal area. Lefsky (2002) developed one single equation that was able to relate canopy structure with AGB in a temperate deciduous, temperate coniferous and boreal coniferous site.

A limitation with transferring our equation would be the underestimation of the canopy height model. Although the slope coefficient may not be significantly different, if not for the underestimation, the coefficient of the constant would be biased to our study site; therefore, an accurate CHM would be required to ensure optimal results for transferability. One of the challenges with using structural variables is the task of building an accurate DTM, and in turn, generating an accurate CHM (Baltsavias, 1999; van Iersel et al., 2017). UAVs using an optical sensor are unable to penetrate beneath the understory vegetation, therefore, finding ground points can be difficult. If an accurate DTM cannot be generated for a site, biomass cannot be accurately measured using structural variables.

3.5.3.2 Significance of research/future applications

The results collected from this research demonstrate the capabilities of UAVs in capturing low-stature shrubs in dense conditions. Mapping shrubs, or low-stature vegetation, is challenging with remote sensing because high resolution imagery is required. Our study demonstrates that a UAV with a consumer-grade camera is able to locate and quantify shrubs as small as 1m in height. Figure 3.9 shows an ortho-image of a willow before and after harvesting. We were able to add to this body of research by demonstrating that UAVs can also be used to measure the biomass of shrubs in a peatland site.

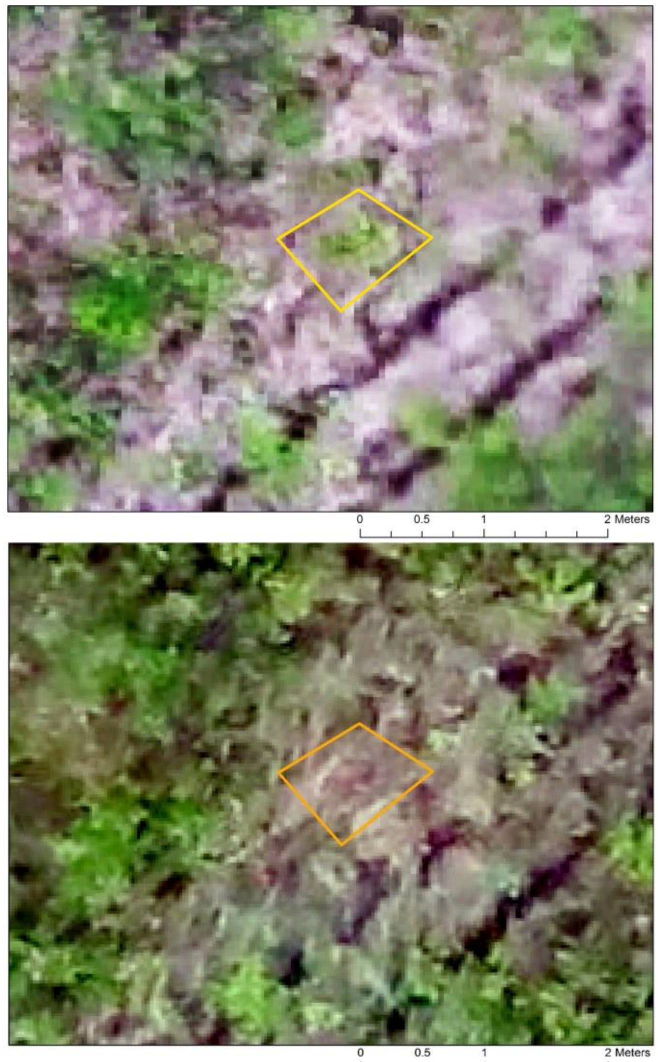

Figure 3.9: *Orthoimages of before (top) and after (bottom) harvesting of a 1.2 m tall willow*

3.6 Conclusion

The main objectives of this research paper was to 1) compare the performance of spectral and structural variables for estimating shrubby AGB and 2) to produce a high-quality map of AGB shrub biomass across our 2-ha study area. The comparison of our ten structural and spectral variables demonstrated that structural variables performed significantly better than spectral variables. All structural variables had a $R^2 > 0.594$ whereas all spectral variables had a $R^2 < 0.274$. UAV-volume was the best predictor of AGB with a R^2 of 0.86, also outperforming the field-measured variables where R^2 values ranged from 0.417 – 0.740. The UAV-volume variable was used as the predictor variable for AGB and applied to all shrubs in the study area.

One of the main challenges, in the creation of the AGB map, was generating an accurate DTM, which is the foundation for generating an accurate CHM. The site is densely vegetated with high volumes of grasses and sedges. We found that our CHM was systematically underestimating the height of the shrubs and attributed the sensor's inability to penetrate past the grass layer as the reason for the error. However, because this was a systematic error and not a random error, it did not significantly influence or affect the accuracy of our AGB equation. Our equation was able to accurately estimate biomass of shrubs in our site, however, the portability of this equation into other sites have remain unassessed.

This study is the first biomass estimation study undertaken in peatlands using UAVs. We have demonstrated that UAVs are not only able to capture low stature shrubs (< 1 m in height) but that they can be used to estimate individual shrub biomass using volumetric information. The UAV platform was able to offer the high-resolution imagery required to face the challenges associated with mapping low-lying shrubs. Our site had the additional advantage of only being composed of three dominant shrub species which had also been found, in a previous research paper, to not be structurally different from each other. Other researchers that use this method may have the additional challenge of having to identify species and applying species-specific equations.

3.7 References

Abdollahnejad, A., Panagiotidis, D., & Surový, P. (2018). Estimation and Extrapolation of Tree Parameters Using Spectral Correlation between UAV and Pléiades Data. *Forests*, *9*(2), 85.

Adkinson, A. C., Syed, K. H., & Flanagan, L. B. (2011). Contrasting responses of growing season ecosystem CO2 exchange to variation in temperature and water table depth in two peatlands in northern Alberta, Canada. *Journal of Geophysical Research: Biogeosciences*, *116*(G1).

Anderson, J. E., Plourde, L. C., Martin, M. E., Braswell, B. H., Smith, M. L., Dubayah, R. O., ... & Blair, J. B. (2008). Integrating waveform lidar with hyperspectral imagery for inventory of a northern temperate forest. *Remote Sensing of Environment*, *112*(4), 1856-1870.

Asner, G. P., Hughes, R. F., Varga, T. A., Knapp, D. E., & Kennedy-Bowdoin, T. (2009). Environmental and biotic controls over aboveground biomass throughout a tropical rain forest. *Ecosystems*, *12*(2), 261-278.

Baltsavias, E. P. (1999). A comparison between photogrammetry and laser scanning. *ISPRS Journal of photogrammetry and Remote Sensing*, *54*(2-3), 83-94.

Bendig J., Bolten A., Bennertz S., Broscheit J., Eichfuss S., Bareth G. (2014). Estimating biomass of barley using Crop Surface Models (CSMs) derived from UAV-based RGB imaging. *Remote Sens.* 610395–10412. 10.3390/rs61110395

Bendig, J., Yu, K., Aasen, H., Bolten, A., Bennertz, S., Broscheit, J., ... & Bareth, G. (2015). Combining UAV-based plant height from crop surface models, visible, and near infrared vegetation indices for biomass monitoring in barley. *International Journal of Applied Earth Observation and Geoinformation*, *39*, 79-87.

Blackburn, G. A., & Steele, C. M. (1999). Towards the remote sensing of matorral vegetation physiology: Relationships between spectral reflectance, pigment, and biophysical characteristics of semiarid bushland canopies. *Remote sensing of Environment*, *70*(3), 278-292.

Blodau, C. and Siems, M.: Drainage-induced forest growth alters belowground carbon biogeochemistry in the Mer Bleue bog, Canada, Biogeochemistry, 107, 107–123, 2012

Boegh, E., Soegaard, H., Broge, N., Hasager, C. B., Jensen, N. O., Schelde, K., & Thomsen, A. (2002). Airborne multispectral data for quantifying leaf area index, nitrogen concentration, and photosynthetic efficiency in agriculture. *Remote sensing of Environment*, *81*(2-3), 179-193.

Bona, K. A., Hilger, A., Burgess, M., Wozney, N., & Shaw, C. (2018). A peatland productivity and decomposition parameter database. *Ecology*, *99*(10), 2406-2406.

Brand, G. J., & Smith, W. B. (1985). Evaluating allometric shrub biomass equations fit to generated data. *Canadian Journal of Botany*, *63*(1), 64-67.

Camill, P., Lynch, J. A., Clark, J. S., Adams, J. B., & Jordan, B. (2001). Changes in biomass, aboveground net primary production, and peat accumulation following permafrost thaw in the boreal peatlands of Manitoba, Canada. *Ecosystems*, *4*(5), 461-478.

Campbell, C., Vitt, D. H., Halsey, L. A., Campbell, I. D., Thormann, M. N., & Bayley, S. E. (2000). Net primary production and standing biomass in northern continental wetlands. *Information Report-Northern Forestry Centre, Canadian Forest Service*, (NOR-X-369).

Chen, J. M. (1996). Evaluation of vegetation indices and a modified simple ratio for boreal applications. *Canadian Journal of Remote Sensing*, *22*(3), 229-242.

Chen, Q., Gong, P., Baldocchi, D., & Tian, Y. Q. (2007). Estimating basal area and stem volume for individual trees from lidar data. *Photogrammetric Engineering & Remote Sensing*, *73*(12), 1355-1365.

Chen, Q., Laurin, G. V., Battles, J. J., & Saah, D. (2012). Integration of airborne lidar and vegetation types derived from aerial photography for mapping aboveground live biomass. *Remote Sensing of Environment*, *121*, 108-117.

Clark, M. L., Roberts, D. A., Ewel, J. J., & Clark, D. B. (2011). Estimation of tropical rain forest aboveground biomass with small-footprint lidar and hyperspectral sensors. *Remote Sensing of Environment*, *115*(11), 2931-2942.

Connolly, B. J., & Grigal, D. F. (1983). Biomass estimation equations for wetland tall shrubs.

Couwenberg, J., Thiele, A., Tanneberger, F., Augustin, J., Bärisch, S., Dubovik, D., ... & Joosten, H. (2011). Assessing greenhouse gas emissions from peatlands using vegetation as a proxy. *Hydrobiologia*, *674*(1), 67-89.

Dandois, J. P., & Ellis, E. C. (2013). High spatial resolution three-dimensional mapping of vegetation spectral dynamics using computer vision. *Remote Sensing of Environment*, *136*, 259-276.

Dong, J., Kaufmann, R. K., Myneni, R. B., Tucker, C. J., Kauppi, P. E., Liski, J., ... & Hughes, M. K. (2003). Remote sensing estimates of boreal and temperate forest woody biomass: carbon pools, sources, and sinks. *Remote Sensing of Environment*, *84*(3), 393-410.

Du, H., Cui, R., Zhou, G., Shi, Y., Xu, X., Fan, W., & Lü, Y. (2010). The responses of Moso bamboo (Phyllostachys heterocycla var. pubescens) forest aboveground biomass to Landsat TM spectral reflectance and NDVI. *Acta Ecologica Sinica*, *30*(5), 257-263.

Englhart, S., Keuck, V., & Siegert, F. (2011). Aboveground biomass retrieval in tropical forests—The potential of combined X-and L-band SAR data use. *Remote sensing of environment*, *115*(5), 1260-1271.

Estornell, J., Ruiz, L. A., Velázquez-Martí, B., & Fernández-Sarría, A. (2011). Estimation of shrub biomass by airborne LiDAR data in small forest stands. *Forest Ecology and Management*, *262*(9), 1697-1703.

Foody, G. M., Boyd, D. S., & Cutler, M. E. (2003). Predictive relations of tropical forest biomass from Landsat TM data and their transferability between regions. *Remote sensing of environment*, *85*(4), 463-474.

Fraser, R. H., Olthof, I., Lantz, T. C., & Schmitt, C. (2016). UAV photogrammetry for mapping vegetation in the low-Arctic. *Arctic Science*, *2*(3), 79-102.

Gao, X., Huete, A. R., Ni, W., & Miura, T. (2000). Optical–biophysical relationships of vegetation spectra without background contamination. *Remote Sensing of Environment*, *74*(3), 609-620.Boegh et al., 2002

Gasparri, N. I., Parmuchi, M. G., Bono, J., Karszenbaum, H., & Montenegro, C. L. (2010). Assessing multi-temporal Landsat 7 ETM+ images for estimating above-ground biomass in subtropical dry forests of Argentina. *Journal of Arid Environments*, *74*(10), 1262-1270.

Gasparri, N. I., Parmuchi, M. G., Bono, J., Karszenbaum, H., & Montenegro, C. L. (2010). Assessing multi-temporal Landsat 7 ETM+ images for estimating above-ground biomass in subtropical dry forests of Argentina. *Journal of Arid Environments*, *74*(10), 1262-1270.

Gerylo, G. R., Hall, R. J., Franklin, S. E., & Smith, L. (2002). Empirical relations between Landsat TM spectral response and forest stands near Fort Simpson, Northwest Territories, Canada. *Canadian Journal of Remote Sensing*, *28*(1), 68-79.

Gleason, C. J., & Im, J. (2011). A review of remote sensing of forest biomass and biofuel: options for small-area applications. *GIScience & Remote Sensing*, *48*(2), 141-170.

Goodbody, T. R., Coops, N. C., Marshall, P. L., Tompalski, P., & Crawford, P. (2017). Unmanned aerial systems for precision forest inventory purposes: A review and case study. *The Forestry Chronicle*, *93*(1), 71-81.

Greaves, H. E., Vierling, L. A., Eitel, J. U., Boelman, N. T., Magney, T. S., Prager, C. M., & Griffin, K. L. (2016). High-resolution mapping of aboveground shrub biomass in Arctic tundra using airborne lidar and imagery. *Remote Sensing of Environment*, *184*, 361-373.

Hall, R. J., Skakun, R. S., Arsenault, E. J., & Case, B. S. (2006). Modeling forest stand structure attributes using Landsat ETM+ data: Application to mapping of aboveground biomass and stand volume. *Forest ecology and management*, *225*(1-3), 378-390.

Hame, T., Salli, A., Andersson, K., & Lohi, A. (1997). A new methodology for the estimation of biomass of coniferdominated boreal forest using NOAA AVHRR data. *International Journal of Remote Sensing*, *18*(15), 3211-3243.

He, A., McDermid, G., Rahman, M., Strack, M., Saraswati, S., & Xu, B. (2018). Developing Allometric Equations for Estimating Shrub Biomass in a Boreal Fen. Forests, 9(9), 569.

Hird, J. N., Montaghi, A., McDermid, G. J., Kariyeva, J., Moorman, B. J., Nielsen, S. E., & McIntosh, A. (2017). Use of unmanned aerial vehicles for monitoring recovery of forest vegetation on petroleum well sites. *Remote Sensing*, *9*(5), 413.

IPCC, (2007). Impacts, Adaptation and Vulnerability: Contribution of working group II to the fourth assessment report of the inter-governmental panel on climate change, edited by: Parry, M. L., Canziani, O. F., Palutikof, J. P., van der Linden, P. J., and Hanson, C. E., Cambridge University Press, Cambridge, United King-dom, 976 pp.

Jakubauskas, M. E., & Price, K. P. (1997). Empirical relationships between structural and spectral factors of Yellowstone lodgepole pine forests. Photogrammetric Engineering and Remote Sensing, 63, 1375−1381

Kachamba, D. J., Ørka, H. O., Gobakken, T., Eid, T., & Mwase, W. (2016). Biomass estimation using 3D data from unmanned aerial vehicle imagery in a tropical woodland. *Remote Sensing*, *8*(11), 968.

Kellndorfer, J. M., Walker, W. S., LaPoint, E., Kirsch, K., Bishop, J., & Fiske, G. (2010). Statistical fusion of Lidar, InSAR, and optical remote sensing data for forest stand height characterization: A regional-scale method based on LVIS, SRTM, Landsat ETM+, and ancillary data sets. *Journal of Geophysical Research: Biogeosciences*, *115*(G2).

Kellndorfer, J., Walker, W., Pierce, L., Dobson, C., Fites, J. A., Hunsaker, C., ... & Clutter, M. (2004). Vegetation height estimation from shuttle radar topography mission and national elevation datasets. *Remote sensing of Environment*, *93*(3), 339-358.

Korrensalo, A., Kettunen, L., Laiho, R., Alekseychik, P., Vesala, T., Mammarella, I., & Tuittila, E. S. (2018). Boreal bog plant communities along a water table gradient differ in their standing biomass but not their biomass production. *Journal of Vegetation Science, 29*(2), 136-146.

Labrecque, S., Fournier, R. A., Luther, J. E., & Piercey, D. (2006). A comparison of four methods to map biomass from Landsat-TM and inventory data in western Newfoundland. *Forest Ecology and Management*, *226*(1-3), 129-144.

Lappalainen, E. (Ed.). (1996). *Global peat resources* (Vol. 4, p. 358). Jyskä: International Peat Society.

Laurin, G. V., Chen, Q., Lindsell, J. A., Coomes, D. A., Del Frate, F., Guerriero, L., ... & Valentini, R. (2014). Above ground biomass estimation in an African tropical forest with lidar and hyperspectral data. *ISPRS Journal of Photogrammetry and Remote Sensing, 89*, 49-58.

Lefsky, M. A., Cohen, W. B., Acker, S. A., Parker, G. G., Spies, T. A., & Harding, D. (1999). Lidar remote sensing of the canopy structure and biophysical properties of Douglas-fir western hemlock forests. *Remote sensing of environment*, *70*(3), 339-361.

Lefsky, M. A., Cohen, W. B., Harding, D. J., Parker, G. G., Acker, S. A., & Gower, S. T. (2002). Lidar remote sensing of above-ground biomass in three biomes. *Global ecology and biogeography*, *11*(5), 393-399.

Li, H., Mausel, P., Brondizio, E., & Deardorff, D. (2010). A framework for creating and validating a non-linear spectrum-biomass model to estimate the secondary succession biomass in moist tropical forests. *ISPRS Journal of Photogrammetry and Remote Sensing*, *65*(2), 241-254.

Lim, K., Treitz, P., Baldwin, K., Morrison, I., & Green, J. (2003). Lidar remote sensing of biophysical properties of tolerant northern hardwood forests. *Canadian Journal of Remote Sensing*, *29*(5), 658-678.

Limpens, J., Berendse, F., Blodau, C., Canadell, J. G., Freeman, C., Holden, J., ... & Schaepman-Strub, G. (2008). Peatlands and the carbon cycle: from local processes to global implications-a synthesis. *Biogeosciences*, *5*, 1475-1491.

Lovitt, J., Rahman, M. M., & McDermid, G. J. (2017). Assessing the value of UAV photogrammetry for characterizing terrain in complex peatlands. *Remote Sensing*, *9*(7), 715.

Lu, D. (2006). The potential and challenge of remote sensing-based biomass estimation. *International journal of remote sensing*, *27*(7), 1297-1328.

Lu, D., & Batistella, M. (2005). Exploring TM image texture and its relationships with biomass estimation in Rondônia, Brazilian Amazon. *Acta Amazonica*, *35*(2), 249-257.

Lu, D., Chen, Q., Wang, G., Liu, L., Li, G., & Moran, E. (2016). A survey of remote sensing-based aboveground biomass estimation methods in forest ecosystems. *International Journal of Digital Earth*, *9*(1), 63-105.

Lu, D., Chen, Q., Wang, G., Moran, E., Batistella, M., Zhang, M., ... & Saah, D. (2012). Aboveground forest biomass estimation with Landsat and LiDAR data and uncertainty analysis of the estimates. *International Journal of Forestry Research, 2012*.

Lu, D., Mausel, P., Brondızio, E., & Moran, E. (2004). Relationships between forest stand parameters and Landsat TM spectral responses in the Brazilian Amazon Basin. *Forest ecology and management*, *198*(1-3), 149-167.

Lucas, N. S., Curran, P. J., Plummer, S. E., & Danson, F. M. (2000). Estimating the stem carbon production of a coniferous forest using an ecosystem simulation model driven by the remotely sensed red edge. *International Journal of Remote Sensing*, *21*(4), 619-631.

Lucas, R. M., Mitchell, A. L., & Armston, J. (2015). Measurement of forest above-ground biomass using active and passive remote sensing at large (subnational to global) scales. *Current Forestry Reports*, *1*(3), 162-177.

Lucas, R. M., Mitchell, A. L., Rosenqvist, A. K. E., Proisy, C., Melius, A., & Ticehurst, C. (2007). The potential of L-band SAR for quantifying mangrove characteristics and change: case studies from the tropics. *Aquatic conservation: marine and freshwater ecosystems*, *17*(3), 245-264.

Madec, S., Baret, F., De Solan, B., Thomas, S., Dutartre, D., Jezequel, S., ... & Comar, A. (2017). High-throughput phenotyping of plant height: comparing Unmanned Aerial Vehicles and ground LiDAR estimates. *Frontiers in plant science, 8.*

Main-Knorn, M., Cohen, W. B., Kennedy, R. E., Grodzki, W., Pflugmacher, D., Griffiths, P., & Hostert, P. (2013). Monitoring coniferous forest biomass change using a Landsat trajectory-based approach. *Remote Sensing of Environment*, *139*, 277-290.

Mercer, J. J., & Westbrook, C. J. (2016). Ultrahigh-resolution mapping of peatland microform using ground-based structure from motion with multiview stereo. *Journal of Geophysical Research: Biogeosciences*, *121*(11), 2901-2916.

Munir, T.M., Xu, B., Perkins, M., and M. Strack. (2014). Responses of carbon dioxide flux and plant biomass to water table drawdown in a treed peatland in northern Alberta: a climate change perspective. Biogeosciences, 11, 807-820.

Mutanga, O., & Skidmore, A. K. (2004). Narrow band vegetation indices overcome the saturation problem in biomass estimation. *International Journal of Remote Sensing*, *25*(19), 3999-4014.

Mutanga, O., Adam, E., & Cho, M. A. (2012). High density biomass estimation for wetland vegetation using WorldView-2 imagery and random forest regression algorithm. *International Journal of Applied Earth Observation and Geoinformation, 18,* 399-406.

Næsset, E., & Gobakken, T. (2008). Estimation of above- and below-ground biomass across regions of the boreal forest zone using airborne laser. Remote Sensing of Environment, 112, 3079–3090.

Næsset, E., & Gobakken, T. (2008). Estimation of above-and below-ground biomass across regions of the boreal forest zone using airborne laser. *Remote Sensing of Environment*, *112*(6), 3079-3090.

Natural Regions Committee. (2006). Natural regions and subregions of Alberta. *Government of Alberta*

Natural Resources Canada. *(*2018). 8 facts about Canada's boreal forest. *Government of Canada*

Olsoy, P. J., Glenn, N. F., Clark, P. E., & Derryberry, D. R. (2014). Aboveground total and green biomass of dryland shrub derived from terrestrial laser scanning. *ISPRS Journal of Photogrammetry and Remote Sensing*, *88*, 166-173.

Ota T., Ogawa M., Shimizu K., Kajisa T., Mizoue N., Yoshida S., et al. (2015). Aboveground biomass estimation using structure from motion approach with aerial photographs in a seasonal tropical forest. *Forests* 6 3882–3898. 10.3390/f6113882

Ota, T., Ogawa, M., Mizoue, N., Fukumoto, K., & Yoshida, S. (2017). Forest Structure Estimation from a UAV-Based Photogrammetric Point Cloud in Managed Temperate Coniferous Forests. *Forests*, *8*(9), 343.

Peregon, A., & Yamagata, Y. (2013). The use of ALOS/PALSAR backscatter to estimate above-ground forest biomass: A case study in Western Siberia. *Remote Sensing of Environment*, *137*, 139-146.

Popescu, S. C., Wynne, R. H., & Scrivani, J. A. (2004). Fusion of small-footprint lidar and multispectral data to estimate plot-level volume and biomass in deciduous and pine forests in Virginia, USA. *Forest Science*, *50*(4), 551-565.

Powell, S. L., Cohen, W. B., Healey, S. P., Kennedy, R. E., Moisen, G. G., Pierce, K. B., & Ohmann, J. L. (2010). Quantification of live aboveground forest biomass dynamics with Landsat time-series and field inventory data: A comparison of empirical modeling approaches. *Remote Sensing of Environment*, *114*(5), 1053-1068.

Puliti, S., Ørka, H. O., Gobakken, T., & Næsset, E. (2015). Inventory of small forest areas using an unmanned aerial system. *Remote Sensing*, *7*(8), 9632-9654.

Rahman, M. M., McDermid, G. J., Strack, M., & Lovitt, J. (2017). A new method to map groundwater table in peatlands using unmanned aerial vehicles. *Remote Sensing*, *9*(10), 1057.

Repola, J. (2009). Biomass equations for Scots pine and Norway spruce in Finland.

Robinson, S. D., & Moore, T. R. (2000). The influence of permafrost and fire upon carbon accumulation in high boreal peatlands, Northwest Territories, Canada. *Arctic, Antarctic, and Alpine Research*, *32*(2), 155-166.

Seidel, D., Fleck, S., Leuschner, C., & Hammett, T. (2011). Review of ground-based methods to measure the distribution of biomass in forest canopies. *Annals of Forest Science*, *68*(2), 225-244.

Soenen, S. A., Peddle, D. R., Hall, R. J., Coburn, C. A., & Hall, F. G. (2010). Estimating aboveground forest biomass from canopy reflectance model inversion in mountainous terrain. *Remote Sensing of Environment*, *114*(7), 1325-1337.

Solberg, S., Astrup, R., Gobakken, T., Næsset, E., & Weydahl, D. J. (2010). Estimating spruce and pine biomass with interferometric X-band SAR. *Remote Sensing of Environment*, *114*(10), 2353-2360.

Steininger, M. K. (2000). Satellite estimation of tropical secondary forest above-ground biomass: data from Brazil and Bolivia. *International Journal of Remote Sensing*, *21*(6-7), 1139-1157.

Sturm, P., & Triggs, B. (1996, April). A factorization based algorithm for multi-image projective structure and motion. In *European conference on computer vision* (pp. 709-720). Springer, Berlin, Heidelberg.

Swain, K. C., Thomson, S. J., & Jayasuriya, H. P. (2010). Adoption of an unmanned helicopter for low-altitude remote sensing to estimate yield and total biomass of a rice crop. *Transactions of the ASABE*, *53*(1), 21-27.

Tarnocai, C. (2006). The effect of climate change on carbon in Canadian peatlands. *Global and planetary Change*, *53*(4), 222-232.

Tarnocai, C., Canadell, J. G., Schuur, E. A. G., Kuhry, P., Mazhitova, G., & Zimov, S. (2009). Soil organic carbon pools in the northern circumpolar permafrost region. *Global biogeochemical cycles*, *23*(2).

Tilly N., Aasen H., Bareth G. (2015). Fusion of plant height and vegetation indices for the estimation of barley biomass. *Remote Sens.* 7 11449–11480. 10.3390/rs70911449

Turner, D. P., Cohen, W. B., Kennedy, R. E., Fassnacht, K. S., & Briggs, J. M. (1999). Relationships between leaf area index and Landsat TM spectral vegetation indices across three temperate zone sites. *Remote sensing of environment*, *70*(1), 52-68.

van Iersel, W., Straatsma, M., Addink, E., & Middelkoop, H. (2018). Monitoring height and greenness of non-woody floodplain vegetation with UAV time series. *ISPRS Journal of Photogrammetry and Remote Sensing*, *141*, 112-123.

Vitt, D. H., Wieder, R. K., Scott, K. D., & Faller, S. (2009). Decomposition and peat accumulation in rich fens of boreal Alberta, Canada. *Ecosystems*, *12*(3), 360-373.

Walker, W. S., Kellndorfer, J. M., LaPoint, E., Hoppus, M., & Westfall, J. (2007). An empirical InSAR-optical fusion approach to mapping vegetation canopy height. *Remote Sensing of Environment*, *109*(4), 482-499.

Wieder, R. K., Vitt, D. H., & Benscoter, B. W. (2006). Peatlands and the boreal forest. In *Boreal peatland ecosystems* (pp. 1-8). Springer, Berlin, Heidelberg.

Yin X., McClure M. A., Jaja N., Tyler D. D., Hayes R. M. (2011). In-season prediction of corn yield using plant height under major production systems. *Agron. J.* 103:92310.2134/agronj2010.0450

Yue, J., Yang, G., Li, C., Li, Z., Wang, Y., Feng, H., & Xu, B. (2017). Estimation of winter wheat above-ground biomass using unmanned aerial vehicle-based snapshot hyperspectral sensor and crop height improved models. *Remote Sensing*, *9*(7), 708.

Zhang, G., Ganguly, S., Nemani, R. R., White, M. A., Milesi, C., Hashimoto, H., ... & Myneni, R. B. (2014). Estimation of forest aboveground biomass in California using canopy height and leaf area index estimated from satellite data. *Remote Sensing of Environment*, *151*, 44-56.

Zhang, J. (2010). Multi-source remote sensing data fusion: status and trends. *International Journal of Image and Data Fusion*, *1*(1), 5-24.

Zheng, D., Rademacher, J., Chen, J., Crow, T., Bresee, M., Le Moine, J., & Ryu, S. R. (2004). Estimating aboveground biomass using Landsat 7 ETM+ data across a managed landscape in northern Wisconsin, USA. *Remote sensing of environment*, *93*(3), 402-411.

Zolkos, S. G., Goetz, S. J., & Dubayah, R. (2013). A meta-analysis of terrestrial aboveground biomass estimation using lidar remote sensing. *Remote Sensing of Environment*, *128*, 289-298

Chapter Four: Summary and Conclusions

This thesis aimed to develop methods to map shrubby AGB in a peatland. Regional AGB estimates provide valuable information to assess greenhouse gas emissions which has become increasingly important with the rising threat of climate change. Substantial research has, therefore, gone into developing biomass estimation models. Despite the vast literature, very few studies are found for peatlands; specifically quantifying the multi-stemmed shrub species that can dominate various peatland types (e.g. fens). The research presented here aimed to address this knowledge gap by presenting the results of two biomass estimation studies undertaken in a boreal continental fen using two approaches: 1) field-based method through the development of allometric equations, and 2) remote-sensing method using UAV-photogrammetry. Research into optimizing remote sensing methods has become popular because remote sensing offers data over large scales that field-based are unable to offer. However, field-based methods are the most accurate method in estimating biomass (Lu et al., 2016) and field-based measurements are required to validate and calibrate remote sensing methods. The results from Chapter 2 were used in the experimental design and analysis to obtain the results for Chapter 3.

4.1 Research Objectives Summary

The two objectives that were addressed in the studies were:

1. To develop allometric equations for dominant shrub species found in a boreal continental fen.
    a. Assess the portability of previously published allometric equations for the same shrub species.
    b. Assess the need for genus-specific equations

2. To assess the capacity of UAV photogrammetry for mapping aboveground biomass in a boreal continental fen
    a. Compare the relative value of spectral and structural variables for measuring shrubby AGB
    b. Create an AGB map of shrub biomass of the study area using the best predictor variable.

To address each specific objective below:

- (Objective 1a) We compared our locally developed phylogenetic equations with three external sources and found that all equations, with the exception of one, were significantly different. This result suggests that site-specific equations are required and that allometric relationships are influenced by site conditions.
- (Objective 1b) Three genus-specific equations and one generalized equation were developed for dominant shrub species found in peatlands ($R^2 > 0.91$). The generalized equation was determined to not be significantly different from each genus-specific equation which lead to the conclusion that shrubs, regardless of genus, followed similar allometry rates.
- (Objective 2a) In order to assess the capacity of UAV photogrammetry to measure AGB, ten spectral and structural variables were tested to determine the best-performing predictor variable for AGB. Similar to other studies (Clark et al., 2011; Tilley et al., 2015), we found that structural variables performed significantly better than the chosen spectral variables (e.g. vegetation indices). Vegetation indices are known to have low data saturation points (Lu et al. ,2015; Bendig et al., 2015), and because our study site is densely vegetated, this could explain the poor performance of the VIs in predicting AGB.

- (Objective 2b) Volume was the variable chosen to be used in the AGB map with a R^2 of 0.86 and RMSE of 500.33g. The UAV-measured volume also performed better than the field measured variables (height, width, and volume) which had a R^2 ranging from 0.417 – 0.740 and RMSE ranging from 744.34g – 1126.76g. Object-based image analysis was used to identify shrubs from other landcover features (e.g. water and grass). The generated confusion matrix showed that the overall classification accuracy was 79.33%. The volumetric AGB equation was cross validated and applied to all shrub objects across the site. The sum of all shrub biomass values reported a total estimated biomass value of 53 854.2 kg with a mean average error of 421.05g across the 2-ha site.

4.2 Research Contributions/Application

Peatlands represent a significant sink in the global carbon cycle and accurate biomass estimates for these ecoregions are required to calculate global carbon balances. Despite their global importance, peatlands have previously been excluded from studies (Hame et al., 1997) because of the complexity involved with mapping the dwarf shrubs. Chapter 2 and Chapter 3 represent two studies using two different biomass estimation techniques applied to a peatland site.

Within the allometric literature, only three studies were found where allometric equations were developed for the dominant shrub species found in our study site. Two out of the three studies were in wetland sites and both were published prior to 1985. He et al., (2018), or Chapter 2 of this thesis, is the first-known study that developed allometric equations for dominant shrub species in a northern Albertan peatland. In addition, the conclusion that a generalized equation is sufficient in measuring shrub biomass is important for future allometric studies. The discussion of generalized equations is commonly found across allometric studies and the results from this study add to this body of research (e.g. Buech & Rigg, 1989 and Mosseler et al., 2016). The use of one general equation compared to developing genus-specific equations can significantly reduce the fieldwork and destructive sampling required for allometric studies and other biomass estimation studies as well. For example, in Chapter 3, one volumetric equation was used to estimate the biomass of all shrub species based on the conclusions made in Chapter 2. The task of species classification, using remote sensing, would have required significantly more data processing and could also introduce classification errors.

Chapter 3 will also be the first-known study that used UAV- measured variables to estimate biomass across a peatland site. UAVs have become more popular in the biomass estimation literature; however, they have not been tested in peatland sites. Chapter 3 demonstrates the capabilities of UAVs in being able to map shrub biomass that spaceborne sensors have previously been unable to successfully map (Hame et al., 1997; Nelson et al 2010). Our research also demonstrated the suitability of a volumetric variable in estimating AGB. Other lidar studies have used crown geometric volume as a proxy for estimating basal area and stem volume (Chen et al., 2007), however we did not find any studies that used our method to calculate volume from a UAV.

Other contributions include:

1. Select material from Chapter 2 and 3 was presented at the Linear Disturbances in Peatland Workshop
2. Select material from Chapter 2 was presented in the form of a poster at the COSIA 2018 conference

3. Select material from Chapter 3 was presented in the form of a poster at the Ecological Society of America (ESA) 2018 conference.
4. The published manuscript arising from Chapter 2 (He et al., 2018) represents a formal contribution to the literature.
5. A manuscript arising from Chapter 3 is expected to be submitted to the journal *Remote Sensing*.

4.3 Recommendations for Future Research

4.3.1 Portability of allometric and volume-based equations

The equations, reported in Chapter 2 and Chapter 3, were sufficient in estimating biomass in the study region where they were developed. However, we did not assess the portability of these equations into other peatland sites. The development of allometric equations and the volume-AGB equation required destructive sampling and was time-intensive, therefore understanding the extent to which equations can be applied is valuable. Previous allometric studies found that the inclusion of samples from different study sites would assist with increasing the portability of equations (Muukkonen, 2007; Case & Hall, 2008). Our locally derived equations may be biased towards site-specific conditions, therefore, more samples from other sites are required to increase portability. Regional biomass estimates are becoming increasingly important, therefore efforts in developing generalized equations to estimate biomass is valuable. The reduction of field work and the development of equations can be very beneficial for future biomass estimation studies.

4.3.2 Assessing the use of volume in other ecoregions

Our research marks one instance where UAV- derived volume performed well in estimating AGB. Future research into the performance of this variable in other ecoregions could be a valuable contribution to the biomass estimation literature. The diversity in genus and size on our site is not as diverse in comparison to other ecoregions; our study site had 3 shrub genera that ranged between 50cm – 3m in height. It would be interesting to assess whether volume-based equations will still perform well in ecoregions with a higher biodiversity and to what degree of accuracy.

4.3.3 Optimization of the classification of landcover type

Spectral bands, with the addition of CHM, were used in the image segmentation and classification process. The thresholds used to segment and classify the image (see Figure 3.5) were configured through trial-and-error by visually assessing the orthophotograph. The spectral values were not corrected into reflectance values; therefore, the same thresholds would produce different classification accuracies in other images because of varying illumination conditions. Future studies may want to optimize the classification process by using reflectance values instead of radiance values. This optimization would most valuable in cases where multiple images are being used; it would decrease the time required in manually adjusting thresholds.

Chapter Five: Bibliography

Alberta Energy. (2011). What is Oil Sands. Available at https://www.energy.alberta.ca/OS/AOS/Pages/FAS.aspx (accessed 27 August 2018).

Alberta Environment and Sustainable Resource Development (ESRD). 2015. Alberta Wetland Classification System. Water Policy Branch, Policy and Planning Division, Edmonton, AB.

Alberta Environment and Parks (AEP). (2014). Assessing Wetlands in Alberta. Available at http://aep.alberta.ca/water/programs-and-services/wetlands/default.aspx (accessed 22 November 2018).

Bartsch, I., & Moore, T. R. (1985). A preliminary investigation of primary production and decomposition in four peatlands near Schefferville, Québec. *Canadian Journal of Botany*, *63*(7), 1241-1248.

Bendig J., Bolten A., Bennertz S., Broscheit J., Eichfuss S., Bareth G. (2014). Estimating biomass of barley using Crop Surface Models (CSMs) derived from UAV-based RGB imaging. *Remote Sens.* 610395–10412. 10.3390/rs61110395

Bendig, J., Yu, K., Aasen, H., Bolten, A., Bennertz, S., Broscheit, J., ... & Bareth, G. (2015). Combining UAV-based plant height from crop surface models, visible, and near infrared vegetation indices for biomass monitoring in barley. *International Journal of Applied Earth Observation and Geoinformation*, *39*, 79-87.

Bond-Lamberty, B., Wang, C., & Gower, S. T. (2002). Aboveground and belowground biomass and sapwood area allometric equations for six boreal tree species of northern Manitoba. *Canadian Journal of Forest Research*, *32*(8), 1441-1450.

Brand, G. J., & Smith, W. B. (1985). Evaluating allometric shrub biomass equations fit to generated data. *Canadian Journal of Botany*, *63*(1), 64-67.

Braverman, M., & Quinton, W. L. (2016). Hydrological impacts of seismic lines in the wetland-dominated zone of thawing, discontinuous per-mafrost, Northwest Territories, Canada. Hydrological Processes, 30,2617–2627. https://doi.org/10.1002/hyp.10695

Bridgham, S. D., Cadillo-Quiroz, H., Keller, J. K., & Zhuang, Q. (2013). Methane emissions from wetlands: biogeochemical, microbial, and modeling perspectives from local to global scales. *Global change biology*, *19*(5), 1325-1346.

Brinson, M. M., Lugo, A. E., & Brown, S. (1981). Primary productivity, decomposition and consumer activity in freshwater wetlands. *Annual Review of Ecology and Systematics*, *12*(1), 123-161.

Campbell, C., Vitt, D. H., Halsey, L. A., Campbell, I. D., Thormann, M. N., & Bayley, S. E. (2000). Net primary production and standing biomass in northern continental wetlands. *Information Report-Northern Forestry Centre, Canadian Forest Service*, (NOR-X-369).

Case, B. S., & Hall, R. J. (2008). Assessing prediction errors of generalized tree biomass and volume equations for the boreal forest region of west-central Canada. *Canadian Journal of Forest Research*, *38*(4), 878-889.

Chapman, S., Buttler, A., Francez, A. J., Laggoun-Défarge, F., Vasander, H., Schloter, M., ... & Gilbert, D. (2003). Exploitation of northern peatlands and biodiversity maintenance: a conflict between economy and ecology. *Frontiers in Ecology and the Environment*, *1*(10), 525-532.

Carlson, M., Chen, J., Elgie, S., Henschel, C., Montenegro, Á., Roulet, N., ... & Wells, J. (2010). Maintaining the role of Canada's forests and peatlands in climate regulation. *The Forestry Chronicle*, *86*(4), 434-443.

Charman, D. (2002). *Peatlands and environmental change*. John Wiley & Sons Ltd.

Christensen, J. H., Hewitson, B., Busuioc, A., Chen, A., Gao, X., Held, R., ... & Magaña Rueda, V. (2007). Regional climate projections. In *Climate Change, 2007: The Physical Science Basis. Contribution of Working group I to the Fourth Assessment Report of the Intergovernmental Panel on Climate Change, University Press, Cambridge, Chapter 11*(pp. 847-940).

Clark, D. B., & Kellner, J. R. (2012). Tropical forest biomass estimation and the fallacy of misplaced concreteness. *Journal of Vegetation Science*, *23*(6), 1191-1196.

Cleary, J., Roulet, N. T. & Moore, T. R. Greenhouse gas emissions from Canadian peat extraction. 1990–2000: a life-cycle analysis. Ambio 34, 456–461 (2005).

Connolly, B. J., & Grigal, D. F. (1983). Biomass estimation equations for wetland tall shrubs.

Couwenberg, J., Thiele, A., Tanneberger, F., Augustin, J., Bärisch, S., Dubovik, D., ... & Joosten, H. (2011). Assessing greenhouse gas emissions from peatlands using vegetation as a proxy. *Hydrobiologia*, *674*(1), 67-89

Crawford, T. M., & Bluestein, H. B. (2000). An operational, diagnostic surface energy budget model. *Journal of Applied Meteorology*, *39*(7), 1196-1217.

Dias, A. T., Hoorens, B., Van Logtestijn, R. S., Vermaat, J. E., & Aerts, R. (2010). Plant species composition can be used as a proxy to predict methane emissions in peatland ecosystems after land-use changes. *Ecosystems*, *13*(4), 526-538.

Ducks Unlimited. (2015). Boreal Wetland Fact Sheets. Accessed on September 25 2018. Accessed from http://www.ducks.ca/assets/2015/09/Boreal-Wetlands-Fact-Sheets.pdf

Englhart, S., Keuck, V., & Siegert, F. (2011). Aboveground biomass retrieval in tropical forests—The potential of combined X-and L-band SAR data use. *Remote sensing of environment*, *115*(5), 1260-1271.

Fargione, J., Hill, J., Tilman, D., Polasky, S., & Hawthorne, P. (2008). Land clearing and the biofuel carbon debt. *Science*, *319*(5867), 1235-1238.

Fraser, R. H., Olthof, I., Lantz, T. C., & Schmitt, C. (2016). UAV photogrammetry for mapping vegetation in the low-Arctic. *Arctic Science*, *2*(3), 79-102.

Gillies, C. (2011). Water management techniques for resource roads in wetlands: A state of practice review. *FPInnovations Contract Report for Ducks Unlimited Canada CR-652*.

Gleason, C. J., & Im, J. (2011). A review of remote sensing of forest biomass and biofuel: options for small-area applications. *GIScience & Remote Sensing*, *48*(2), 141-170.

Government of Alberta. (2012). Lower Athabasca regional plan 2012–2022.

Hame, T., Salli, A., Andersson, K., & Lohi, A. (1997). A new methodology for the estimation of biomass of coniferdominated boreal forest using NOAA AVHRR data. *International Journal of Remote Sensing*, *18*(15), 3211-3243.

Hansen, M. C., Stehman, S. V., & Potapov, P. V. (2010). Quantification of global gross forest cover loss. *Proceedings of the National Academy of Sciences*, *107*(19), 8650-8655.

Hengeveld, H. G. (2000). Projections for Canada's climate future. *Climate change digest*, *500*, 1-27.

He, A., McDermid, G., Rahman, M., Strack, M., Saraswati, S., & Xu, B. (2018). Developing Allometric Equations for Estimating Shrub Biomass in a Boreal Fen. *Forests*, *9*(9), 569.

Hopkinson, C., Chasmer, L. E., Sass, G., Creed, I. F., Sitar, M., Kalbfleisch, W., & Treitz, P. (2005). Vegetation class dependent errors in lidar ground elevation and canopy height estimates in a boreal wetland environment. *Canadian Journal of Remote Sensing*, *31*(2), 191-206.

Intergovernmental Panel on Climate Change (IPCC). (2007). *Climate change 2007: contribution of... to the fourth assessment report of the Intergovernmental Panel on Climate Change. 2. Impacts, adaptation and vulnerability: contribution of Working Group II to the fourth assessment report of the Intergovernmental Panel on Climate Change*. Cambridge University Press.

Joabsson, A., Christensen, T. R., & Wallén, B. (1999). Vascular plant controls on methane emissions from northern peatforming wetlands. *Trends in Ecology & Evolution*, *14*(10), 385-388.

Knox, S. H., Sturtevant, C., Matthes, J. H., Koteen, L., Verfaillie, J., & Baldocchi, D. (2015). Agricultural peatland restoration: effects of land-use change on greenhouse gas (CO2 and CH4) fluxes in the Sacramento-San Joaquin Delta. *Global change biology*, *21*(2), 750-765.

Kulawardhana, R. W., Popescu, S. C., & Feagin, R. A. (2014). Fusion of lidar and multispectral data to quantify salt marsh carbon stocks. Remote Sensing of Environment, 154, 345-357

Kuzyakov, Y., & Gavrichkova, O. (2010). Time lag between photosynthesis and carbon dioxide efflux from soil: a review of mechanisms and controls. *Global Change Biology*, *16*(12), 3386-3406.

Lai, D. Y. F. (2009). Methane dynamics in northern peatlands: a review. *Pedosphere*, *19*(4), 409-421.

Le Toan, T., Quegan, S., Davidson, M. W. J., Balzter, H., Paillou, P., Papathanassiou, K., ... & Ulander, L. (2011). The BIOMASS mission: Mapping global forest biomass to better understand the terrestrial carbon cycle. *Remote sensing of environment*, *115*(11), 2850-2860.

Lieffers, V. J., & Rothwell, R. L. (1987). Rooting of peatland black spruce and tamarack in relation to depth of water table. *Canadian Journal of Botany*, *65*(5), 817-821.

Lieffers, V. J., & Macdonald, S. E. (1990). Growth and foliar nutrient status of black spruce and tamarack in relation to depth of water table in some Alberta peatlands. *Canadian Journal of Forest Research*, *20*(6), 805-809.

Lovitt, J., Rahman, M. M., Saraswati, S., McDermid, G. J., Strack, M., & Xu, B. (2018). UAV Remote Sensing Can Reveal the Effects of Low‐Impact Seismic Lines on Surface Morphology, Hydrology, and Methane (CH4) Release in a Boreal Treed Bog. *Journal of Geophysical Research: Biogeosciences*, *123*(3), 1117-1129.

Lu, D. (2006). The potential and challenge of remote sensing‐based biomass estimation. *International journal of remote sensing*, *27*(7), 1297-1328.

Lu, D., Chen, Q., Wang, G., Liu, L., Li, G., & Moran, E. (2016). A survey of remote sensing-based aboveground biomass estimation methods in forest ecosystems. *International Journal of Digital Earth*, *9*(1), 63-105.

Lucas, R. M., Mitchell, A. L., & Armston, J. (2015). Measurement of forest above-ground biomass using active and passive remote sensing at large (subnational to global) scales. *Current Forestry Reports*, *1*(3), 162-177.

Miller, C. A., Benscoter, B. W., & Turetsky, M. R. (2015). The effect of long-term drying associated with experimental drainage and road construction on vegetation composition and productivity in boreal fens. *Wetlands ecology and management*, *23*(5), 845-854.

Moore, T. R., & Dalva, M. (1993). The influence of temperature and water table position on carbon dioxide and methane emissions from laboratory columns of peatland soils. *Journal of Soil Science*, *44*(4), 651-664.

Moore, T. R., Roulet, N. T., & Waddington, J. M. (1998). Uncertainty in predicting the effect of climatic change on the carbon cycling of Canadian peatlands. *Climatic change*, *40*(2), 229-245.

Moore, T. R., Trofymow, J. A., Taylor, B., Prescott, C., Camire, C., Duschene, L., ... & Siltanen, M. (1999). Litter decomposition rates in Canadian forests. *Global Change Biology*, *5*(1), 75-82.

Mora, C., Vieira, G., Pina, P., Lousada, M., & Christiansen, H. H. (2015). Land cover classification using high-resolution aerial photography in adventdalen, svalbard. *Geografiska Annaler: Series A, Physical Geography*, *97*(3), 473-488.

Muukkonen, P. (2007). Generalized allometric volume and biomass equations for some tree species in Europe. *European Journal of Forest Research*, *126*(2), 157-166.

Munir, T. M., Xu, B., Perkins, M., & Strack, M. (2014). Responses of carbon dioxide flux and plant biomass to water table drawdown in a treed peatland in northern Alberta: a climate change perspective.

Mutanga, O., & Skidmore, A. K. (2004). Narrow band vegetation indices overcome the saturation problem in biomass estimation. *International Journal of Remote Sensing*, *25*(19), 3999-4014.

National Wetlands Working Group (NWWG). (1997). *The Canadian Wetland Classification.* Environment Canada

Natural Regions Committee. (2006). Natural regions and subregions of Alberta. *Compiled by DJ Downing and WW Pettapiece. Government of Alberta. Pub*.

Nelson, R. (2010). Model effects on GLAS-based regional estimates of forest biomass and carbon. *International Journal of Remote Sensing*, *31*(5), 1359-1372.

Pasher, J., Seed, E., & Duffe, J. (2013). Development of boreal ecosystem anthropogenic disturbance layers for Canada based on 2008 to 2010 Landsat imagery. *Canadian Journal of Remote Sensing*, *39*(1), 42-58.

Patterson L & Cooper DJ. 2007. Wetlands, 27, 290-304.

Paul, K. I., Roxburgh, S. H., England, J. R., Ritson, P., Hobbs, T., Brooksbank, K., ... & Neumann, C. (2013). Development and testing of allometric equations for estimating above-ground biomass of mixed-species environmental plantings. *Forest Ecology and Management*, *310*, 483-494.

Peregon, A., & Yamagata, Y. (2013). The use of ALOS/PALSAR backscatter to estimate above-ground forest biomass: A case study in Western Siberia. *Remote Sensing of Environment*, *137*, 139-146.

Puliti, S., Ørka, H. O., Gobakken, T., & Næsset, E. (2015). Inventory of small forest areas using an unmanned aerial system. *Remote Sensing*, *7*(8), 9632-9654.

Schaudt, K. J., & Dickinson, R. E. (2000). An approach to deriving roughness length and zero-plane displacement height from satellite data, prototyped with BOREAS data. *Agricultural and Forest Meteorology*, *104*(2), 143-155.

Shi, X., Thornton, P. E., Ricciuto, D. M., Hanson, P. J., Mao, J., Sebestyen, S. D., ... & Bisht, G. (2015). Representing northern peatland microtopography and hydrology within the Community Land Model. *Biogeosciences Discussions (Online)*, *12*(4).

Silvola, J., Alm, J., Ahlholm, U., Nykanen, H., & Martikainen, P. J. (1996). CO_2 fluxes from peat in boreal mires under varying temperature and moisture conditions. *Journal of ecology*, 219-228.

Song, C. (2013). Optical remote sensing of forest leaf area index and biomass. *Progress in Physical Geography*, *37*(1), 98-113.

Strack, M., Waddington, J. M., Rochefort, L., & Tuittila, E. S. (2006). Response of vegetation and net ecosystem carbon dioxide exchange at different peatland microforms following water table drawdown. *Journal of Geophysical Research: Biogeosciences*, *111*(G2).

Strack, M. (Ed.). (2008). Peatlands and Climate Change. Saarijärvi, FIN: International Peat Society(IPS).

Strack, M., Softa, D., Bird, M., & Xu, B. (2018). Impact of winter roads on boreal peatland carbon exchange. *Global change biology*, *24*(1), e201-e212.System. (2nd ed.). Waterloo, ON: University of Waterloo

Tarnocai, C. (2006). The effect of climate change on carbon in Canadian peatlands. *Global and planetary Change*, *53*(4), 222-232.

Tarnocai, C. (2009). The impact of climate change on Canadian peatlands. *Canadian Water Resources Journal*, *34*(4), 453-466.

Tarnocai, C., I.M. Kettles and B. Lacelle. (2011). Peatlands of Canada; Geological Survey of Canada, Open File 6561 (digital database); CD-ROM.

Tømmervik, H., Karlsen, S. R., Nilsen, L., Johansen, B., Storvold, R., Zmarz, A., ... & Zagajewski, B. (2014). Use of unmanned aircraft systems (UAS) in a multi-scale vegetation index study of arctic plant communities in Adventdalen on Svalbard.

Turetsky, M. R., Donahue, W. F., & Benscoter, B. W. (2011). Experimental drying intensifies burning and carbon losses in a northern peatland. *Nature Communications*, *2*, 514.

Turetsky, M.R., Kotowska, A., Bubier, J., Dise, N.B., Crill, P., Hornibrook, E.R.C., … Wilmking,M. (2014). A synthesis of methane emissions from 71 northern, temperate, and subtropical wetlands. Global Change Biology, 20, 2183-2197.

Van Rensen, C. K., Nielsen, S. E., White, B., Vinge, T., & Lieffers, V. J. (2015). Natural regeneration of forest vegetation on legacy seismic lines in boreal habitats in Alberta's oil sands region. *Biological Conservation*, *184*, 127-135.

Verwijst, T., & Telenius, B. (1999). Biomass estimation procedures in short rotation forestry. *Forest Ecology and Management*, *121*(1-2), 137-146.

Vitt, D. H. (2006). Functional characteristics and indicators of boreal peatlands. In *Boreal peatland ecosystems* (pp. 9-24). Springer, Berlin, Heidelberg.

Vitt, D. H., Halsey, L. A., Bauer, I. E., & Campbell, C. (2000). Spatial and temporal trends in carbon storage of peatlands of continental western Canada through the Holocene. *Canadian Journal of Earth Sciences*, *37*(5), 683-693.

Vitt, D. H., Wieder, R. K., Scott, K. D., & Faller, S. (2009). Decomposition and peat accumulation in rich fens of boreal Alberta, Canada. *Ecosystems*, *12*(3), 360-373.

Wieder, R. K., Vitt, D. H., & Benscoter, B. W. (2006). Peatlands and the boreal forest. In *Boreal peatland ecosystems* (pp. 1-8). Springer, Berlin, Heidelberg.

Wieder, R. K., Scott, K. D., Kamminga, K., Vile, M. A., Vitt, D. H., Bone, T., ... & Bhatti, J. S. (2009). Postfire carbon balance in boreal bogs of Alberta, Canada. *Global Change Biology*, *15*(1), 63-81.

Wuebbles, D. J., & Hayhoe, K. (2002). Atmospheric methane and global change. *Earth-Science Reviews*, *57*(3-4), 177-210.

Yeh, S., Jordann, S., Brandt, A., & Spatari, S. (2009). Land use Greenhouse Gas Emissions for conventional and unconventional oil production. *UC Davis Institute for transportation studies (extended abstract) UCD-ITS-RR-09-04 Available at http://steps. ucdavis. edu/People/slyeh/syeh-resources/uc-lcfs/Fossil% 20fuel*, *20*, l.

Yu, Z (2012). Northern peatland carbon stocks and dynamics: a review. Biogeosciences 9:4071-4085

Yue, J., Yang, G., Li, C., Li, Z., Wang, Y., Feng, H., & Xu, B. (2017). Estimation of winter wheat above-ground biomass using unmanned aerial vehicle-based snapshot hyperspectral sensor and crop height improved models. *Remote Sensing*, *9*(7), 708.

Zolkos, S. G., Goetz, S. J., & Dubayah, R. (2013). A meta-analysis of terrestrial aboveground biomass estimation using lidar remote sensing. *Remote Sensing of Environment*, *128*, 289-298.